The Shannon Information Capacity of an Arbitrary Radiating Surface: An Electromagnetic Approach

Said Mikki

***Abstract*— Utilizing a cross-disciplinary approach, we explore Shannon information-theoretic characterizations of the information capacity limits of generic electromagnetic (EM) surfaces intended for possible use in wireless communication links. Our principal task is to first formulate at a general and rigorous level the EM theory of the information that can be extracted from the Maxwellian fields radiated by an arbitrarily shaped continuous surface. This is then followed by a detailed derivation and illustration of practical physics-informed algorithms for computing approximations of the Shannon capacity of surfaces with any given geometry operating in Gaussian channels. Our formalism can address both near- and far-field information capacity scenarios, with a mathematical treatment that includes a complete characterization of the source-field polarization structure, mutual coupling, and interactions.**

***Index Terms*— Antenna theory, capacity limits, electromagnetic (EM) theory, information theory.**

NOMENCLATURE

$\mathbf{A}$	Vector in $\mathbb{R}^3$.
$\overline{\mathbf{A}}$	Dyad in $\mathbb{R}^3$.
$\mathbf{A}\cdot\mathbf{B}$	Vector–vector inner product in $\mathbb{R}^3$.
$\overline{\mathbf{A}}\cdot\mathbf{B}$	Dyad–vector product in $\mathbb{R}^3$.
$\overline{A}$	Column array of arbitrary length.
$\overline{\overline{A}}$	2-D array (matrix) of arbitrary size.
$\overline{\overline{A}}\cdot\overline{B}$	Matrix–column array product.
$\overline{\overline{A}}\cdot\overline{\overline{B}}$	Matrix–matrix array product.
$\mathbf{A}\otimes\mathbf{B}$	Vector–vector tensor product.
$\overline{\overline{A}}^{\dagger}$, $\overline{\mathbf{A}}^{\dagger}$	Hermitian operation of a matrix or dyad.
$\overline{\overline{A}}^{T}$, $\overline{\mathbf{A}}^{T}$	Transpose operation of a matrix or dyad.
$\|\overline{\overline{A}}\|_F$, $\|\overline{\mathbf{A}}\|_F$	Frobenius norm of a matrix or dyad.

I. INTRODUCTION

THE subject matter of this article belongs to the electromagnetic (EM) theory of information, a topic that while not totally new as such [1], [2] is currently reemerging into multiple fields [3], [4], [5], [6], [7], [8], [9]. This is an interdisciplinary discourse cutting through both EM and information theory, where there has been an interest in synthesizing selected ideas taken from EM theory, EM engineering, information theory, system theory, communication theory, and signal processing, by coherently integrating them into one or few closely related formalisms in which both information and physical degrees of freedom are subjected to careful evaluation, analysis, and manipulation at the same theoretical and computational technical levels [10]. In the EM theory of information, it appears that there are three major research problems, namely, statistical correlation processes, often manifest at microscopic or local levels [11], [12], [13], [14], [15], [16], [17]; system representations of continuous phenomena, where the objective is to devise exact and rigorous signal processing models of physical fields [18], [19], [20]; and mutual information in wave processes [18], especially characteristics most commonly seen at the global level of point-to-point or end-to-end link capacity [21], for example, using the popular degree-of-freedom approach [5], [22]. Our main focus in this article is on the third major problem in the EM theory of information, i.e., that of the physics-informed approach to the analysis, understanding, and use of capacity concepts. This subject has numerous applications. For example, a physics-based take on information capacity may open the door for new ideas in conventional Shannon theory by introducing applications outside coding and error-correction methodologies [18]. Also, an EM understanding of capacity can lead to a better understanding (and hence design) of the overall communication link by injecting EM knowledge into the signal processing part [23]. Perhaps the most obvious example of such potential is the recent interest in capacity-driven optimization and design of various systems [24], [25], [26], [27], [28].

To present a concrete contribution, we further restrict our attention to a specific type of information transmitting systems, EM surfaces, but we try to maintain as much generality in the definition of such structures as possible. The idea of a radiating or transmitting surface is fundamental in different fields. Indeed, the concept encompasses a diverse range of problems and applications; for example, the following conditions hold:

1) In antenna and scattering theories, with the use of the surface equivalence theorem, it is possible to show that any radiating structure whatsoever can be modeled as a system of surface current distributions [29], [30].
2) Intelligent transmitting surfaces to be deployed as large-and-complex EM surface structures mounted in

Manuscript received 2 May 2022; revised 23 November 2022; accepted 4 December 2022. Date of publication 9 January 2023; date of current version 6 March 2023.

The author is with the Zhejiang University/University of Illinois at Urbana–Champaign (ZJU-UIUC) Institute, Zhejiang University, International Campus, Haining, Zhejiang 314400, China (e-mail: said.m.mikki@gmail.com).

Color versions of one or more figures in this article are available at https://doi.org/10.1109/TAP.2023.3234164.

Digital Object Identifier 10.1109/TAP.2023.3234164

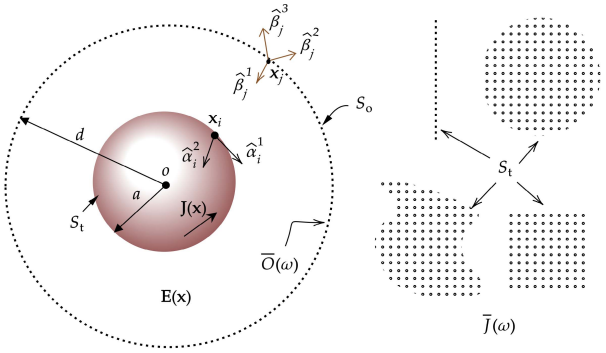

Fig. 1. Left: example of a transmitting spherical continuous surface S_t with observation (receiving) system comprised of another spherical surface S_o accessed by a measuring apparatus $\mathcal{S}_o$. Right: examples of several discrete N_t-approximations of transmitting surfaces with various 3-D geometrical shapes giving rise to the discrete current distribution source model $\bar{J}(\omega)$.

dense and dynamic wireless communication environments intended to control and improve the network performance by injecting new signals into the channel for use in information transmission, estimation, or testing.

3) Reconfigurable reflecting EM surfaces, often operated in scattering modes, are deployed in order to control and modify the prorogation characteristics of complex and unpredictable media, especially as envisioned for the forthcoming 6G technology [31], [32], [33], [34].

In such applications (and others not discussed here), a generic transmitting surface S_t may be viewed as an artificial active or passive "EM source" assigned the task of contributing information to the communication channel, whether in the form of an individual concrete antenna element, a continuous distribution of transmitting sources, or reconfigurable reflector. The unifying concept here is that the surface is a continuous EM source conformal to a geometrically shaped two-manifold where we find that both EM and geometrical degrees of freedom inextricably coupled together. On the other hand, in information theory, capacity and entropy concepts have been mostly developed for point-to-point communication schemes where the dominant mathematical model is the random variable and the random process [35]. Unfortunately, a continuous EM source requires a random field theory [36] for its proper mathematical treatment [37]. To the best of our knowledge, a complete and fully rigorous stochastic calculus theory of the Maxwellian field suitable for the purpose of communication system analysis has not been constructed yet.[1] To evade this shortcoming, in this article, we propose a computational approach that can be used to approximate fundamental capacity limits of arbitrarily shaped EM surfaces under quite generic statistical scenarios.

[1]However, there have been several attempts to study various aspects of the EM problem from the statistical viewpoint, e.g., random media, propagation modes in fluctuating domains, and channel models in wireless networks [38], [39], [40]. Nevertheless, we do not consider most of these theories proper stochastic calculus theories. In the latter case, the very differential and integral operators themselves must be replaced by stochastic generalizations [41], where it turns out that the rules of ordinary calculus in Maxwell's theory may not apply [42].

There are three major theoretical considerations that must be considered while attempting to build a satisfactory EM theory of information for radiating surfaces. We mention here that some of what the author believes is currently the most urgent.

1) The information capacity of a surface would, in general, depend on how the latter's radiated fields are measured. The measurement apparatus is formally analogous to a receiver system in wireless communication systems.
2) The information capacity of a continuous source supported by a surface S_t depends on the purely geometrical features of the surface as encoded by its Riemannian structure, i.e., the local metric relations and how they vary from one point on the surface to another. In addition, the attained capacity depends on other physical parameters such as the electrical area (size) of the surface (physical area normalized with respect to the wavelength).
3) The information capacity depends on the type of the radiated field, i.e., whether near or far fields, distance of the observation system to the source, and the radiation fields' rich polarization and wavelength substructures.

We believe that these problems and the related considerations have not received sufficient attention in the sprawling literature on EM capacity. In fact, capacity studies tend to be approached from the perspective of rather specific examples and systems, hence sometimes avoiding the most general formulation possible for the sake of concreteness. In our approach, we intentionally try to keep the discussion as general and fundamental as possible while carefully addressing each of the abovementioned physics-based contributions to the purely information-theoretic definition of capacity. Our strategy is based on identifying and isolating a proper physical structure—whether geometrical or EM—that dominates a corresponding information-theoretic aspect of the overall system. However, we use a computational approach where eventually a concrete (still general) algorithm for computing capacity electromagnetically is devised and illustrated with several examples. The proposed method is suitable for integration with standard full-wave EM solvers, especially the method of moment (MoM) [43].

This article is organized as follows. In Section II, we provide a broad outline of the rather general (and very complex) problem of describing the information-theoretic setting of the EM communication system in space–time. The purpose is to motivate the need for our alternative (simpler) strategy, which is to be developed in the following. We begin formulating the latter (computational) approach in Section III, where the key necessary mathematical ideas of the frequency-domain formalism, based on the deployment of a hierarchy of finite point dipole model approximations, is outlined. Formulas for the information capacity are then derived in Section IV for the ubiquitous additive white Gaussian noise (AWGN) model. Extensive numerical examples and analysis are then provided in Section V,[2] followed by conclusion. A series of

[2]These examples focus on the fundamental aspects of our algorithm and the theory behind it. For future work, a fuller analysis of the impact of depolarization and diffraction's effects on the information capacity may be helpful (e.g., wave scattering off buildings and other scatterers and antennas).

supporting appendixes is also inserted at the end to complete the presentation found in the main part of this article.

II. Fundamental Considerations

Imagine a generic EM transmitting system represented by a radiating surface S_t endowed with the structure of a differentiable (smooth) manifold. Without loss of generality, one may take these two-surface to be a perfectly electric conductor (PEC), but the following formulation can be extended to more generic EM boundary conditions. We assume that an information source system is modeled as $\mathcal{S} = \{s_i,\, i \in I\}$, where s_i is a random variable whose probability distribution is $p_i(s)$ and I is an index set (could be finite, countable, or uncountable). Each random variable s_i might be discrete or continuous though we focus on the continuous case in the following. One way of thinking about the signal s_i is that it represents the information symbols injected into a "point port" of the continuous surface S_t (see the following). Our main objective of this article is to investigate the information capacity of the radiating system S_t when connected to (excited by) the information source $\mathcal{S}$.

In the standard setting of classical EM systems, i.e., the regime where macroscopic Maxwell's equations hold [44], information may be injected into the device only through specialized structures called ports [29], [45]. These are waveguide structures capable of confining EM fields across the transverse plane, while energy flows along the waveguide axis [46]. For simplicity, we assume that at each port, only one waveguide field mode (the dominant mode) is excited, which is denoted by $\mathbf{E}_\mathrm{p}^j(\mathbf{x}, t)$, where $\mathbf{x} \in \mathbb{R}^3$ is the position, $t \in \mathbb{R}$ is the time, $j \in \{1, \ldots, N_\mathrm{p}\}$ is the port index, and N_p is the number of point ports. The port excitation field is further assumed to be separable into two main factors, a pure time signal controlled by both the information source and the waveguide field mode's spatial profile. The EM excitation at the jth point port can be written as

$$\mathbf{E}_j^{\mathrm{ex}}(\mathbf{x}, t) = \sum_{n=-\infty}^{\infty} s_{i_{n,j}} u(t - nT_s)\mathbf{E}_\mathrm{p}^j(\mathbf{x}, t). \tag{1}$$

This is the general mathematical model of the information data stream injected into the jth point port. Here, $s_{i_{n,j}}$ is the nth time slot symbol, which is the outcome of the stochastic experiment of drawing from the random variable s_{i_n} when applied to the jth point port. The time pulse $u(t)$ carries information with symbol data rate $f_s = 1/T_s$. In such a model, the map $i_{n,j} : \mathbb{Z} \times \mathbb{N} \to I$ is deployed in order to perform signal multiplexing, so different information symbols $s_i \in \mathcal{S}$ could be transmitted using the same point port if desired.

Let $\overline{\mathbf{F}}_\mathrm{t}(\mathbf{x}, \mathbf{x}'; t, t')$ be the time-dependent current Green's function (2-D tensor of rank 2) of the transmitting surface S_t [7]. The induced surface current due to the jth point port is given by

$$\mathbf{J}_{\mathrm{t},j}(\mathbf{x}, t) = \int_{S_\mathrm{t}} \mathrm{d}^2x' \int_{\mathbb{R}} \mathrm{d}t' \overline{\mathbf{F}}_\mathrm{t}(\mathbf{x}, \mathbf{x}'; t, t') \cdot \mathbf{E}_j^{\mathrm{ex}}(\mathbf{x}', t'). \tag{2}$$

Since the operator relation linking the excitation field and the induced current is linear [47], [48], then the total current due to all point ports exciting the antenna simultaneously is the direct sum of all currents of the form (2), giving rise to [49]

$$\mathbf{J}_\mathrm{t}(\mathbf{x}, t) = \int_{S_\mathrm{t}} \mathrm{d}^2x' \int_{\mathbb{R}} \mathrm{d}t' \overline{\mathbf{F}}_\mathrm{t}(\mathbf{x}, \mathbf{x}'; t, t') \cdot \mathbf{E}^{\mathrm{ex}}(\mathbf{x}', t') \tag{3}$$

where

$$\mathbf{E}^{\mathrm{ex}}(\mathbf{x}', t') = \sum_{j=1}^{N_\mathrm{p}} \sum_{n=-\infty}^{\infty} s_{i_{n,j}} u(t - nT_s)\mathbf{E}_\mathrm{p}^j(\mathbf{x}', t'). \tag{4}$$

The total transmitting current (5) will now radiate into the surrounding space, giving rise to EM fields $\mathbf{E}(\mathbf{x}, t)$ and $\mathbf{H}(\mathbf{x}, t)$. For simplicity, we focus only on the electric field, which can be expressed in terms of the surface current distribution through the following Green's function formula [50], [51]:

$$\mathbf{E}(\mathbf{x}, t) = \int_{S_\mathrm{t}} \mathrm{d}^2x' \int_{\mathbb{R}} \mathrm{d}t' \overline{\mathbf{G}}_0(\mathbf{x}, \mathbf{x}'; t, t') \cdot \mathbf{J}_\mathrm{t}(\mathbf{x}', t'). \tag{5}$$

Here, $\overline{\mathbf{G}}_0$ is the forward electric-field free-space dyadic Green's function (3-D tensor of rank 2), i.e., Green's function of the domain surrounding the antenna where no random scattering objects are assumed to exist [52].

Next, we introduce the surface S_o, which is the two-manifold where observations of the antenna's radiated field will be collected.[3] The received or observed field is the collection

$$\mathcal{O}(S_\mathrm{o}) := \{\mathbf{E}(\mathbf{x}, t) \in \mathbb{R}^3,\, \mathbf{x} \in S_\mathrm{o}\}. \tag{6}$$

Clearly, this is an infinite set, so the problem of estimating a field-theoretic information capacity starting from EM data cannot be dealt with directly using the standard Shannon theory since the latter works best with a finite number of random variable [35], [53].

In order to attain a better conceptual grasp of the general structure of the EM theory of information capacity, we try to capture the essentials of the process of information transmission by a continuous surface S_t as follows:

$$\mathcal{S} \xrightarrow[\text{surface } S_\mathrm{t}]{\text{transmitting}} \mathbf{J}(\mathbf{x}, t) \xrightarrow[\overline{\mathbf{G}}(\mathbf{x},\mathbf{x}',t,t')]{\text{electromagnetic radiation}} \mathbf{E}(\mathbf{x}, t) \xrightarrow[\text{apparatus } S_\mathrm{o}]{\text{observation}} \mathcal{O}. \tag{7}$$

We would like to analyze the information-theoretic structure of the transformation $\mathcal{S} \to \mathcal{O}$. One way to do so is by comparing the Shannon information contents of the two systems comprised of the information source $\mathcal{S}$ and the observation or receiver apparatus $\mathcal{O}$. The most obvious way to do that is through the concept of mutual information between the two random variables [35]. This naturally leads to the relative capacity concept to be defined in detail in Section IV. However, the problem as formulated above is too complex to deal with in such very general form. In Section III, we propose a relatively simpler model where some of the inessential constraints of the general transformation (7) will be relaxed in order to reduce the mathematical complexity of the analysis.

[3]When a full closed manifold S_o is used, the two-manifold S_t is obviously contained inside the volume bounded by S_o. It is such latter scenario what interests us most in this article since it is more fundamental than the transmit–receive scenario in a communication theory where the receiver is localized at a specific spatial region away from the transmitter.

III. Discrete Memoryless Frequency-Domain EM Model and the Approximation Heirarchy

Historically speaking, several methods have been proposed to deal with the information content of continuous classical, quantum, and random fields. Most often, one may first attempt locating a suitable effective Hilbert space representation of the original spatiotemporal classical radiation problem, so the number of degrees of freedom becomes countable, followed by a suitable pragmatic criterion to be employed for truncating the originally infinite dimension to a finite number [18]. Another approach, which we follow here, relies on already starting the description of the problem by reducing the radiating currents and fields themselves to a finite number of elementary excitations or modes (oscillators), which is the method often used in quantum information theory for instance [54], [55].

In the point source approximation hierarchy approach, the number of "point ports" is increased such that, basically, the entire surface S_t is "covered" by excitations. Therefore, our key idea is to replace the infinite number of field-current oscillators in the system $\mathcal{S} \to \mathcal{O}$ by a finite number of oscillators in both sides, namely, N_t at S_t and N_o at S_o, effectively replacing (7) by a scheme in the form $\mathcal{S}(N_\mathrm{t}) \to \mathcal{O}(N_\mathrm{o})$. This basic idea is shown in Fig. 1. In the left panel, we show an illustrative example comprised of a continuous transmitting spherical surface S_t observed by another continuous spherical measurement system S_o. On the right panel, a discretized version of the sphere is shown in addition to some examples of other possible nonspherical geometrical shapes, such as linear, rectangular (patch), and arbitrary-curved radiating surfaces.

In order to perform the calculations in a practical manner, we further restrict ourselves to narrowband signals, so our capacity results will be frequency dependent. To do so, we first need to impose two fundamental assumptions.

1) The transmitting surface port-to-current system is memoryless-in-time, i.e., the following condition holds:
$$\overline{\mathbf{F}}_\mathrm{t}(\mathbf{x}, \mathbf{x}'; t, t') = \overline{\mathbf{F}}_\mathrm{t}(\mathbf{x}, \mathbf{x}'; t - t'). \tag{8}$$
2) The surrounding medium is memoryless-in-time, i.e., shift-invariant or, equivalently
$$\overline{\mathbf{G}}_0(\mathbf{x}, \mathbf{x}'; t, t') = \overline{\mathbf{G}}_0(\mathbf{x}, \mathbf{x}'; t - t'). \tag{9}$$

These two assumptions jointly imply that the communication channel from the source $\mathcal{S}$ to the field $\mathbf{E}(\mathbf{x}, t)$—or the observation set $\mathcal{O}$—is time-invariant. This allows us to use the Fourier transform method and hence work in the frequency domain [49], [56].

Remark 1: It should be noted that in general, the memoryless-in-time current Green's function $\overline{\mathbf{F}}_\mathrm{t}(\mathbf{x}, \mathbf{x}'; t - t')$ is not memoryless-in-space. Indeed, except for quite few and rather uninteresting cases where S_t obeys global spatial translation symmetry, one cannot in general write $\overline{\mathbf{F}}_\mathrm{t}(\mathbf{x}, \mathbf{x}'; t - t') = \overline{\mathbf{F}}_\mathrm{t}(\mathbf{x} - \mathbf{x}'; t - t')$ [19], [49]. Therefore, in terms of the current excitation problem, most radiating structures, e.g., all antennas, do have spatial memory [19], [20]. This is one of the main reasons why a fully fledged spatiotemporal EM theory of information and signal processing is highly nontrivial [7], [10].

In the frequency domain, all dynamic quantities vary sinusoidally in time as per $\exp(-\mathrm{i}\omega t)$, while all fields and currents become complex [29]. Fix a spatiotemporal Fourier mode $\exp(\mathrm{i}\mathbf{k} \cdot \mathbf{x} - \mathrm{i}\omega t)$, where $\mathbf{k}$ is the wavevector. Then, the dispersion relation of the vacuum is $|\mathbf{k}| = k$, where $k = \omega/c$ and c is the speed of light [57]. The dyadic Green's function is given by [52]
$$\begin{aligned}\overline{\mathbf{G}}(\mathbf{x}, \mathbf{x}'; \omega) = {} & \gamma_\omega \frac{1}{\mathrm{i}kR}\big(\overline{\mathbf{I}} - \hat{R} \otimes \hat{R}\big)e^{\mathrm{i}kR} \\ & -\gamma_\omega\left[\frac{1}{(\mathrm{i}kR)^2} - \frac{1}{(\mathrm{i}kR)^3}\right]\big(\overline{\mathbf{I}} - 3\hat{R} \otimes \hat{R}\big)e^{\mathrm{i}kR}\end{aligned} \tag{10}$$
where
$$\gamma_\omega := \frac{-\mu_0 \omega k}{4\pi}, \quad \mathbf{R} := \mathbf{x} - \mathbf{x}', \quad \hat{R} := \frac{\mathbf{R}}{|\mathbf{R}|}. \tag{11}$$
The 3-D tensor $\overline{\mathbf{I}}$ is the unit dyad. The radiated field can be expressed in terms of this Green's function using the formula [51]
$$\mathbf{E}(\mathbf{x}; \omega) = \int_{\mathbf{x}' \in S_\mathrm{t}} \mathrm{d}^2 x' \; \overline{\mathbf{G}}_0(\mathbf{x} - \mathbf{x}', \omega) \cdot \mathbf{J}(\mathbf{x}'; \omega) \tag{12}$$
where in what follows we are interested in the exterior region $\mathbb{R}^3 - S_\mathrm{t} \ni \mathbf{x}$, but the integration is performed over the entire surface $S_\mathrm{t} \ni \mathbf{x}'$.

Our objective is to first construct an algorithm for estimating the capacity of a transmitting surface S_t with respect to an observation surface S_o whose local unit normal vector is $\hat{N}_\mathrm{o}(\mathbf{x}), \mathbf{x} \in S_\mathrm{o}$. There are N_t point sources applied at the transmitting side, where the ith point source is positioned at $\mathbf{x}_i$ while equipped with two polarization degrees of freedom $\hat{\alpha}_i^1$ and $\hat{\alpha}_i^2$ satisfying
$$\hat{\alpha}_i^s \cdot \hat{N}_i = 0, \quad \hat{\alpha}_i^s \cdot \hat{\alpha}_i^{s'} = \delta_{ss'}, \quad \|\hat{\alpha}_i^s\| = 1, \quad s, s' = 1, 2. \tag{13}$$
Here, $\hat{N}_i := \hat{N}_\mathrm{o}(\mathbf{x}_i)$ is the local normal to the surface S_t and $\delta_{ss'}$ is the Kronecker delta function. The following formal characterization of a generic N_t-discretization of the continuous surface S_t is then introduced:
$$\mathcal{S}_\mathrm{t} := \big\{\mathbf{x}_i \in S_\mathrm{t}; \hat{\alpha}_i^s \in \mathbb{R}^3, s = 1, 2\big\}_{i=1}^{N_\mathrm{t}} \tag{14}$$
while $\hat{\alpha}_i^s, s = 1, 2$, are shown in (13). Locally, the current distribution $\mathbf{J}(\mathbf{x}, \omega)$ may be expanded as follows [49], [58]:
$$\mathbf{J}(\mathbf{x}) = \hat{\alpha}^1(\mathbf{x}) J^1(\mathbf{x}) + \hat{\alpha}^2(\mathbf{x}) J^2(\mathbf{x}). \tag{15}$$
Therefore, for a discrete N_t-term point approximation of a generic continuous transmitting current $\mathbf{J}(\mathbf{x})$, we may write
$$\mathbf{J}(\mathbf{x}, \omega; \mathcal{S}_\mathrm{t}) = \sum_{i=1}^{N_\mathrm{t}} \sum_{s=1}^{2} \hat{\alpha}_i^s J_i^s(\omega) \delta(\mathbf{x} - \mathbf{x}_i) \tag{16}$$
where δ is the Dirac delta function (cf. Remark 2). The relation (16) serves as a local expansion of the ith current source on the transmitting surface. Note that $J_i^s(\omega) \in \mathbb{C}$ is a frequency-dependent complex number, while the polarization vectors $\hat{\alpha}_i^s, s = 1, 2$, are frequency-independent [19].

Remark 2: The Dirac delta function in (16) is a surface delta function [59]. The physical dimensions of the current

source amplitudes J_i^s are A · m. Each polarization unit vector $\hat{\alpha}_i^s, i = 1, \ldots, N_\mathrm{t}$ and $s = 1, 2$, is a function of the position $\mathbf{x}_i$. (For simplicity, this is indicated by the use of only the index i.) Such position dependence is essential for the general case since closed curved surfaces in $\mathbb{R}^3$ cannot always be modeled by a single coordinate chart, and hence, the use of local coordinate systems, here exemplified by the expansion (15) of the current into local components along $\hat{\alpha}_i^1$ and $\hat{\alpha}_i^2$, becomes mandatory for a correct treatment of the general case (for more details, see [49], [60]).

Substituting (16) into (12), the following formula is obtained:

$$\mathbf{E}(\mathbf{x}, \omega; \mathcal{S}_\mathrm{t}) = \sum_{i=1}^{N_\mathrm{t}} \sum_{s=1}^{2} \overline{\mathbf{G}}_0(\mathbf{x} - \mathbf{x}_i, \omega) \cdot \hat{\alpha}_i^s J_i^s(\omega). \tag{17}$$

Remark 3: Expression (17) describes the EM field outside S_t and is the key EM model that will be used in this article. It is sometimes referred to in the literature as the infinitesimal dipole model (IDM) and has been successfully utilized in various applications, e.g., see [61], [62], [63], [64], [65], [66]. The relation (17) is valid in both the near- and far-field zones [49], [61], [62] and has been verified extensively both computationally and experimentally [65], [67], [68]. A discrete IDM is known to be singular at the surface S_t itself because Green's functions are themselves singular at $\mathbf{x} = \mathbf{x}'$ [52]. However, in practical computational applications, pertinent to communications and power transfer, one most often works under the condition $\mathbf{x} \neq \mathbf{x}'$ (exterior domain scenario), so the radiated fields as such are never singular [49], [61]. To improve the accuracy of (17) for near-field (NF) predictions, one often needs to increase N_t [66] or use global optimization [62], [65], [69], [70], [71].

The radiated field is observed at the surface S_o, which may or may not fully enclose the radiating surface S_t. If N_o observations points are used to gather field measurements obtained via idealized localized field probes, then the observation system may be described mathematically as the set

$$\mathcal{S}_\mathrm{o} := \left\{\mathbf{x}_j \in S_\mathrm{o}; \hat{\beta}_j^r \in \mathbb{R}^3, r = 1, 2, 3\right\}_{j=1}^{N_\mathrm{o}}. \tag{18}$$

Here, at each $j = 1, \ldots, N_\mathrm{o}$, three perpendicular measurements of the field may be enacted along the three Cartesian directions $\hat{\beta}_j^r, r = 1, 2, 3$.[4]

Remark 4: In general, there is no need to consider observation volumes since it is known from EM theory that the field on a closed surface fully characterizes EM radiation everywhere in space [29]. When the observation surface is not closed, it is possible to use EM machine learning to find an IDM like (16) that can predict the fields everywhere in a suitable domain exterior to the transmitting surface S_t [61], [71], [72].

The signal measured at the jth observation point $\mathbf{x}_j$ along the rth direction at frequency ω is denoted by $O_j^r(\omega) \in \mathbb{C}$. For ideal perfectly localized point probes, this can be given by

$$O_j^r(\omega) = b_j^r(\omega)\, \mathbf{E}(\mathbf{x}_j, \omega; \mathcal{S}_\mathrm{t}) \cdot \hat{\beta}_j^r \tag{19}$$

[4]In other words, each axis triplet $\hat{\beta}_j^r$ can be obtained by a local rotation of the global coordinate system $\hat{x}_r, r = 1, 2, 3$, around the observation point $\mathbf{x}_j$.

where $b_j^r(\omega) \in \mathbb{C}$ is the observation device's adjustable gain or responsitivity function. Substituting (17) into (19), we finally arrive at

$$O_j^r(\omega; \mathcal{S}_\mathrm{t}, \mathcal{S}_\mathrm{o}) = \sum_{i=1}^{N_\mathrm{t}} \sum_{s=1}^{2} b_j^r(\omega)\, \hat{\beta}_j^r \cdot \overline{\mathbf{G}}_0(\mathbf{x}_j - \mathbf{x}_i, \omega) \cdot \hat{\alpha}_i^s \; J_i^s(\omega) \tag{20}$$

for $j = 1, \ldots, N_\mathrm{o}$ and $r = 1, 2, 3$. The expression (20) fully characterizes the observation made at position $\mathbf{x}_j$ along the direction labeled by r when the measurement is conducted over a discretized source $\mathcal{S}_\mathrm{t}$ using the apparatus modeled as $\mathcal{S}_\mathrm{o}$ at frequency ω. One of the merits of (20) is that it allows for the directions of observation measurements, labeled by r and j, to vary locally from position $\mathbf{x}_j$ to position $\mathbf{x}_{j'}$, with also different measurement gain (responsitivity) $b_j^r(\omega)$. In this way, the ability to extract information from the transmitting surface's radiated fields is significantly enhanced.

Next, and motivated by the general formula (20), let us define the matrix element $H_{ij}^{rs} \in \mathbb{C}$ as follows:

$$H_{ij}^{rs}(\omega) := b_j^r(\omega) \hat{\beta}_j^r \cdot \overline{\mathbf{G}}_0(\mathbf{x} - \mathbf{x}_i, \omega) \cdot \hat{\alpha}_i^s \tag{21}$$

with $r = 1, 2, 3$; $s = 1, 2$; $i = 1, \ldots, N_\mathrm{t}$; and $j = 1, \ldots, N_\mathrm{o}$. This is an array of $6N_\mathrm{t}N_\mathrm{o}$ complex numbers that fully characterize EM coupling between the discrete system $\mathcal{S}_\mathrm{t}(N_\mathrm{t})$ and the discrete measurement apparatus $\mathcal{S}_\mathrm{o}(N_\mathrm{o})$. Due to the complexity of formula (21), we may simplify the theory by first isolating those key building blocks giving rise to natural substructures embedded into H_{ij}^{rs}.

We start by looking into how the polarization structure of EM radiation determines the character of the coupling interaction between a radiating source centered at $\mathbf{x}_i$ and observed at $\mathbf{x}_j$. To achieve this, we construct the following matrix relation characterizing the complete EM channel from the ith source to the jth observation point:

$$\overline{O}_j(\omega) = \overline{\overline{H}}_{ij}(\omega) \cdot \bar{J}_i(\omega) \tag{22}$$

for $i = 1, \ldots, N_\mathrm{t}$ and $j = 1, \ldots, N_\mathrm{o}$. The 3×2 matrix $\overline{\overline{H}}_{ij}(\omega)$ is defined as

$$\overline{\overline{H}}_{ij}(\omega) := \begin{bmatrix} H_{ij}^{11}(\omega) & H_{ij}^{12}(\omega) \\ H_{ij}^{21}(\omega) & H_{ij}^{22}(\omega) \\ H_{ij}^{31}(\omega) & H_{ij}^{32}(\omega) \end{bmatrix}_{3\times 2}. \tag{23}$$

On the other hand, the source vector $\bar{J}_i$ possesses two degrees of freedom (surface current source), while the observation array $\overline{O}_j$ is concocted using the radiated field's 3-D data, and hence, it enjoys three degrees of freedom as illustrated by the following array structures:

$$\bar{J}_i(\omega) := \begin{bmatrix} J_i^1(\omega) \\ J_i^2(\omega) \end{bmatrix}, \quad \overline{O}_j(\omega) := \begin{bmatrix} O_j^1(\omega) \\ O_j^2(\omega) \\ O_j^3(\omega) \end{bmatrix}. \tag{24}$$

It should be noted that three degrees of freedom are needed in the NF zone in order to describe the polarization of the EM NF, but this number drops to two in the far zone [73], [74]. This remains true even when the radiating current is always taken as a surface (hence 2-D) distribution as per (15) [75]. Therefore,

the above multidimensional structure is general enough to deal with both near- and far-field information capacity scenarios.

In order to compute the capacity of the entire $\mathcal{S}_t \rightarrow \mathcal{S}_o$ configuration, it is required to assemble all point-to-point interactions of the form (22). First, we build global input and output arrays by a process of concatenating the elementary forms given in (24) as follows:

$$\bar{J}(\omega) := \begin{bmatrix} \bar{J}_1(\omega) \\ \vdots \\ \bar{J}_{N_t}(\omega) \end{bmatrix}_{2N_t \times 1}, \quad \overline{O}(\omega) := \begin{bmatrix} \overline{O}_1(\omega) \\ \vdots \\ \overline{O}_{N_o}(\omega) \end{bmatrix}_{3N_o \times 1}. \tag{25}$$

The complete input-to-output relation of the transmitting surface measurement process can be put into the following matrix form:

$$\overline{O}(\omega) = \overline{\overline{H}}(\omega) \cdot \bar{J}(\omega) \tag{26}$$

where the $\mathcal{S}_t \rightarrow \mathcal{S}_0$ channel matrix is identified as

$$\overline{\overline{H}}(\omega) := \begin{bmatrix} \overline{\overline{H}}_{11}(\omega) & \cdots & \overline{\overline{H}}_{1N_t}(\omega) \\ \vdots & \ddots & \vdots \\ \overline{\overline{H}}_{N_o1}(\omega) & \cdots & \overline{\overline{H}}_{N_oN_t}(\omega) \end{bmatrix}_{3N_o \times 2N_t}. \tag{27}$$

It will be seen in Section IV that the matrix $\overline{\overline{H}}$ in (27) contains an adequate amount of the critical EM data needed for the determination of the information capacity of the generic transmitting surface S_t when the standard random channel model of AWGN is assumed. The key to this result is to note that (26) possesses the same mathematical structure of a typical multi-input–multioutput (MIMO) wireless communication system [40], [76], [77]. The details of such analysis will be presented next.

IV. Information Capacity of Radiating Surfaces

A. Information-Theoretic Background

It can be seen that in our model, information is injected into the generic continuous transmitting surface S_t at N_t points $\mathbf{x}_i$ through the transmitting surface current distribution value $\mathbf{J}(\mathbf{x}_i)$, where each point is associated with two possible independent degrees of freedom labeled by $s = 1, 2$, giving rise to the array $\bar{J}_i$ [see (24)]. The latter can be discrete, continuous, or mixed random vector. For definiteness and to simplify the presentation, we only consider continuous random variables in this article, but the discrete and mixed cases are similar. Overall, this implies that the information content of $\bar{J}(\omega)$, see (25), which is the differential entropy for the continuous random variable case, can be expressed through the formula [53]

$$H(\bar{J}) = -\int_{\bar{J} \in \mathbb{C}^N} \prod_{n=1}^{N} \mathrm{d}^N J_n \; p(J_1, \ldots, J_N) \log p(J_1, \ldots, J_N) \tag{28}$$

where N and $p(J_1, \ldots, J_N)$ are the length and pdf of $\bar{J}$, respectively, while log is the binary logarithm.[5] Standard quantities in information theory, such as the joint entropy $H(\overline{X}, \overline{Y})$, the conditional entropy $H(\overline{X}|\overline{Y})$, and mutual information $H(\overline{X} : \overline{Y})$, may all be defined in a manner analogous to (28) for generic complex random vectors $\overline{X}$ and $\overline{Y}$ [40], [53].

Let the mean value of $\bar{J}$ be $m_{\bar{J}} := \mathbb{E}\{\bar{J}\}$, where $\mathbb{E}$ is the expected value operator. The covariance matrix of the input information vector $\bar{J}$ is the $N \times N$ matrix

$$\overline{\overline{C}}_{\bar{J}} := \mathbb{E}\{(\bar{J} - m_{\bar{J}}) \cdot (\bar{J} - m_{\bar{J}})^\dagger\} \tag{29}$$

where $\dagger$ is the Hermitian operation (complex conjugatation and transpose operations). Note that here, $N = 2N_t$. For the noise part, we consider a complex normal noise vector (circularly symmetric Gaussian) consisting of an $N \times 1$ array $\overline{n}(t) := [n_1(t) \; \ldots \; n_N(t)]^T$, where each element's sample is a zero-mean complex normal random variable, i.e., $n_j(t) \in \mathcal{CN}(0, \sigma_{n_j})$, $j = 1, \ldots, 3N_o$, and all these components are statistically independent [see [40], [78] for details on the mathematical background]. Hence, we have an uncorrelated noise model, which may be put in the form $\overline{n}(t) \in \mathcal{CN}(0, \mathrm{diag}[\sigma_{n_1}, \ldots, \sigma_{n_N}])$. In the AWGN flat-frequency narrowband MIMO model (31), the noise vector has the same length as $\overline{O}$, so here, $N = 3N_o$, while the length of the input (transmitted information) vector $\bar{J}$ is $2N_t$. The power spectral density (PSD) of each Gaussian noise component is flat over its bandwidth with value $\mathcal{N}/2$. The covariance matrix of the noise vector $\overline{n}$ is the $3N_o \times 3N_o$ matrix

$$\overline{\overline{C}}_{\overline{n}} := \mathbb{E}\{(\overline{n} - m_{\overline{n}}) \cdot (\overline{n} - m_{\overline{n}})^\dagger\} = \mathbb{E}\{\overline{n} \cdot \overline{n}^\dagger\} \tag{30}$$

where $m_{\overline{n}}$ is the noise mean vector and is assumed zero.

The AWGN model can be summarized by the following relation:

$$\overline{O}(\omega) = \overline{\overline{H}}(\omega) \cdot \bar{J}(\omega) + \overline{n} \tag{31}$$

where $\overline{n}$ is a sample of the noise vector process introduced above, while $\overline{O}$, $\overline{\overline{H}}$, and $\bar{J}$ are given in (26). In this model, the noise is also assumed to be independent of the information signal $\bar{J}$. We work in a frequency-domain (passband) regime where the carrier (center) frequency is ω, so all these arrays are generally complex.[6] The bandwidth $B := \Delta\omega/2\pi$ around the frequency ω is assumed to be small enough such that the flat-channel approximation can be applied to the noisy MIMO system model (31). Note that there is no loss of generality here since, for wideband channels, one can still use the same model (31) by deploying a suitable orthogonal frequency-division modulation (OFDM) technique [40], [76], [77]. In particular, it was shown recently that specialized EM OFDM schemes can be devised to decouple wideband antenna models where each frequency becomes essentially independent of others [23], [79].

[5] For complex random vectors, the integrals in (28) are to be understood as integrals in the complex plane.

[6] Since the passband and the complex baseband representations are equivalent for the same bandwidth [40], they both yield identical capacity calculations. Note that the EM theory of Section III was developed in the frequency domain with the help of the complex phasor representation of the fields, making it naturally suited for use in conjunction with the complex baseband representation in information theory.

B. Concept of Relative Capacity of a Surface

Throughout the rest of this article, we will be interested in the channel capacity associated with the information transfer process $\mathcal{S}_\mathrm{t} \to \mathcal{S}_\mathrm{o}$, which we define in a way similar to the capacity concept based on reliable communications [35].

Definition 1 (Relative Capacity): If the prior probability of sending a given vector sample of symbols into the N_t radiating point ports $\bar{J}$ is denoted by $p(\bar{J})$, then we define the information capacity of S_t relative to S_o by the formula

$$C_\mathrm{s}(\mathcal{S}_\mathrm{t}, \mathcal{S}_\mathrm{o}) := \max_{p(\bar{J})} I(\bar{J} : \overline{O}) \quad \text{bits/vector-sample} \tag{32}$$

where maximization is performed over all possible vector symbol probability distributions $p(\bar{J})$.

Remark 5: The rigorous and exact definition of relative capacity is given in Definition 1. It is completely determined by the use of a series of well-defined mathematical objects carefully constructed throughout the previous passages of this article, which includes the radiating surface system $\mathcal{S}_\mathrm{t}$ and the measurement apparatus $\mathcal{S}_\mathrm{t}$. The relative capacity measures the information capacity of S_t relative to S_o in the sense that this capacity depends on the geometry of S_t and not on the signal processing details of how the surface was excited. This geometry enters the picture through the channel or coupling matrix $\overline{\overline{H}}$ in (21). The geometry of S_t enters through the local tangential vectors $\hat{\alpha}_i^s$. These local vectors are equivalent to the local Riemannian metric tensor. On the other hand, the relative capacity does not depend on how you code the input signals nor on what the information sent is and so on. This relative capacity is now a property of the surface S_t itself, its radiated fields, and the choice of $\mathcal{S}_\mathrm{o}$.

Recall that mutual information can be expressed as $I(\bar{J} : \overline{O}) = H(\overline{O}) - H(\overline{O}|\bar{J})$. Using (31), this becomes $I(\bar{J} : \overline{O}) = H(\overline{O}) - H(\overline{\overline{H}} \cdot \bar{J} + \overline{n}|\bar{J})$. The origin of information loss is the presence of the noise process $\overline{n}$. Without noise, the capacity is equal to the maximum possible information content of the transmitting surface, which is $H(\bar{J})$. Therefore, knowledge of $\overline{\overline{H}}$ allows the determination of the mutual information and hence capacity. Since the channel matrix (27) is completely determined by the geometry of the transmitting surface and the medium's Green's function, we can then use EM theory to compute approximations of the information capacity of the process $\mathcal{S}_\mathrm{t} \to \mathcal{S}_\mathrm{o}$ as will be shown next. For an AWGN MIMO model such as (31), it has been shown that the capacity per sample is [78]

$$C_\mathrm{s}(\omega) = \log\det\left[\mathbb{1}_N + \overline{\overline{H}}(\omega) \cdot \overline{\overline{C}}_{\bar{J}}(\omega) \cdot \overline{\overline{H}}^\dagger(\omega) \cdot \overline{\overline{C}}_{\overline{n}}^{-1}\right]. \tag{33}$$

Here, det is the matrix determinant operation. The array $\mathbb{1}_N$ is a unit matrix of dimension N, where in the case of (33), we have $N = 3N_\mathrm{o}$.

If the bandwidth of the equivalent baseband channel is B, then the corresponding band-limited signal can be completely recovered with the use of a Nyquist sampling rate of $1/2B$ [80]. Since we assume that the noise PSD is flat over B, i.e., $S_n(f') = \mathcal{N}/2$ for $f' \in [f - B, f + B]$, where $S_n(f')$ is the PSD of the noise signal $n(t)$ around the passband (center) frequency $f = \omega/2\pi$, then the Nyquist samples are uncorrelated [81], which for Gaussian random variables, implies stochastic independence.[7] Therefore, the capacity of the data stream is simply the outcome of the multiplication of the capacity per sample by the data rate, leading to bit/s capacity formula

$$C(\omega) = 2B \log\det\left[\mathbb{1}_{3N_\mathrm{o}} + \overline{\overline{H}}(\omega) \cdot \overline{\overline{C}}_{\bar{J}}(\omega) \cdot \overline{\overline{H}}^\dagger(\omega) \cdot \overline{\overline{C}}_{\overline{n}}^{-1}\right]. \tag{34}$$

Expression (34) provides the most general form of the information capacity in a Gaussian channel setting.

In the following, we examine two possible fundamental scenarios: the first corresponds to the situation when there is no mutual coupling (MC; EM interaction) between the various point sources; the second is the complementary case in which such interactions are present in the transmitting system.

C. No-MC Capacity Formulas

Here, it is assumed that both the signal $\bar{J}$ and the noise $\overline{n}$, when modeled as random vectors, are self-uncorrelated, i.e., their respective covariance matrices take the diagonal form

$$\overline{\overline{C}}_{\bar{J}}(\omega) = \sigma_J^2(\omega)\mathbb{1}_{2N_\mathrm{t}}, \quad \overline{\overline{C}}_{\overline{n}}(\omega) = \sigma_n^2\mathbb{1}_{3N_\mathrm{o}}. \tag{35}$$

This is the most basic scenario in information theory, often referred to in the literature as transmission with no knowledge of the channel state information [76].[8] Substituting (35) into (34) and using a matrix identity,[9] we arrive at

$$C(\omega) = 2B \log\det\left[\mathbb{1}_{2N_\mathrm{t}} + \frac{\sigma_J^2(\omega)}{\sigma_n^2}\overline{\overline{H}}^\dagger(\omega) \cdot \overline{\overline{H}}(\omega)\right], \ \text{bit/s}. \tag{36}$$

The relation (36) is the main capacity formula of the information transmission system $\mathcal{S}_\mathrm{t} \to \mathcal{S}_\mathrm{o}$ when the radiating surface does not possess knowledge of the communication channel. We will, however, work with the following slightly modified version:

$$C(S_\mathrm{t}, S_\mathrm{o}) = 2\log\det\left[\mathbb{1}_{2N_\mathrm{t}} + 3N_\mathrm{o}\rho\overline{\overline{H}}'^\dagger \cdot \overline{\overline{H}}'\right], \ (\text{bit/s/Hz}). \tag{37}$$

The derivation of (37) and the definitions of the normalized channel matrix $\overline{\overline{H}}'$ and the signal-to-noise-ratio ρ can be found in Appendix B. The relation (37) is more convenient for numerical capacity calculations as will be illustrated with several examples in Section V.

[7]The PSD level $\mathcal{N}$ itself may depend on f, i.e., the carrier frequency, but is still required to be constant over the small passband span $2B$ [76], [77].

[8]Since the noise is by assumption a white random process, an explicit dependence of the induced narrowband noise on frequency is not needed here [40], [81], but our model allows for possible variation in $\sigma_J(\omega)$ with respect to the center frequency ω.

[9]Namely, the identity $\det(\mathbb{1}_n + \overline{\overline{A}} \cdot \overline{\overline{B}}) = \det(\mathbb{1}_m + \overline{\overline{B}} \cdot \overline{\overline{A}})$ for $n \times m$ and $m \times n$ matrices $\overline{\overline{A}}$ and $\overline{\overline{B}}$, respectively.

D. EM Coupling and Interactions

MC can affect the achievable data rate and other performance measures in communication systems [8], [24], [49], [82], [83]. This subject will be reexamined here from the fundamental perspective introduced by using an EM approach to information theory. A detailed mathematical analysis of the effect of MC on capacity calculations is outlined in Appendix C using the mathematical apparatus developed in Sections II–IV. We give here the following basic definition and theorem followed by a brief theoretical discussion of the role of EM interactions in information capacity.

Definition 2 (MC in Capacity Calculations): An EM coupling entails that two current source degrees of freedom J_i and $J_{i'}, i \neq i'$, are no longer uncorrelated even if the excitation fields applied at their respective point ports, i.e., E_i^{ex} and $E_{i'}^{\text{ex}}$ in (52), are uncorrelated.

Remark 6: It is possible to reformulate Definition 2 in terms of statistically independent/dependent signals instead of uncorrelated/correlated ones. However, for the EM theory of capacity in Gaussian systems, the correlation approach is sufficient. For other types of channels going beyond the additive Gaussian noise model, stronger versions of Definition 2 might be needed.

Theorem 1 (Condition of No MC): Assume an EM information transmission system $\mathcal{S}_{\text{t}}(N_{\text{t}}) \rightarrow \mathcal{S}_{\text{o}}(N_{\text{o}})$. There is no MC (as defined by Definition 2) in an EM surface S_{t} with current Green's function $\overline{\overline{\mathbf{F}}}(\mathbf{x}, \mathbf{x}', \omega)$ if and only the following conditions holds.

1) *Distinct Ports:*

$$i \neq i' \implies F_{i,i'}^{ss'} = 0. \tag{38}$$

2) *Identical Ports:*

$$i = i', \quad s \neq s' \implies F_{i,i'}^{ss'} = 0 \tag{39}$$

for all $s, s' = 1, 2$ and $i, i' = 1, \ldots, N_{\text{t}}$. Here, $F_{i,i'}^{ss'}$ is defined by (59).

Proof: See Appendix C. □

Remark 7: The condition (39) is included in order to consider the less familiar but perfectly legitimate scenario when two signals are applied at the same point $\mathbf{x}_i \in S_{\text{t}}$ but with MC taking place between the two locally orthogonal current components labeled by $s = 1, 2$. Such coupling may happen not necessarily due to electrical conduction but to slight irregularities in the physical layout leading to NF-to-NF coupling between the two current filaments.

E. EM MC and Mutual Information

In all cases (with or without MC), the joint information content of the transmitting surface S_{t} satisfies

$$H(\bar{J}) = H(\bar{J}, \overline{E}^{\text{ex}}) \tag{40}$$

which is due to the functional relation between the excitation point-port array and the induced current as specified by (58), see Appendix C. Note that this implies $H(\bar{J}|\overline{E}^{\text{ex}}) = 0$, so the mutual information satisfies

$$I(\bar{J} : \overline{E}^{\text{ex}}) := H(\bar{J}) - H(\bar{J}|\overline{E}^{\text{ex}}) = H(\bar{J}) \tag{41}$$

which is consistent with the fact that in our model noise, the only source of information loss is due to thermal noise added at the very end of the observation process as per (31). Hence, no information loss is experienced as we transition from the point-port signal excitation field array $\overline{E}^{\text{ex}}$ to the actual physical radiating current $\bar{J}$. Nevertheless, from the basic information theory, we know that joint information is maximal when all the random variables involved are stochastically independent, where in the latter case, entropy becomes the direct sum of the individual processes [35], [53], that is, we have

$$H(\bar{J}) \leq \sum_{n=1}^{2N_{\text{t}}} H(J_n). \tag{42}$$

However, the theory presented in Appendix C proves the following theorem.

Theorem 2: For an arbitrary spatiotemporal excitation field $\mathbf{E}^{\text{ex}}(\mathbf{x}, \omega)$, however, we sample the radiating current distribution, the obtained current samples $\mathbf{J}_i(\omega)$ in (58) are always correlated if there is MC between the current values obtained at the same sample positions.

Corollary 1: MC (as defined by Definition 2) always leads to a signal correlation matrix $\overline{\overline{C}}_{\bar{J}}(\omega)$ that is nondiagonal.

Proof: This follows immediately from Theorems 1 and 2 and formula (62) in Appendix C. □

It then follows from the above that the information content of the transmitting surface before radiation satisfies the relation

$$H(\bar{J}) \leq \sum_{n=1}^{2N_{\text{t}}} H(J_n; \sigma_{J_n}) \tag{43}$$

where $H(J_n; \sigma_{J_n})$ is the entropy computed using a generalization of assumption (35), namely

$$\overline{\overline{C}}_{\bar{J}}(\omega) = \text{diag}\big[\sigma_{J_1}^2(\omega), \ldots, \sigma_{J_{2N_{\text{t}}}}^2(\omega)\big]. \tag{44}$$

We thus obtain the following corollary.

Corollary 2: A no-mutual-coupling scenario yields an upper bound on the essential amount of information that can be delivered by the transmitting surface's source point-port system before radiation.

This is one reason why the uncoupled diagonal matrix form (44) is considered particularly important in our formulation. On the other hand, after the onset of EM radiation, we move from the radiating current $\bar{J}$ to the radiated field followed by noisy observation $\overline{O}$ as per (31). In contrast to the previous $\overline{E}^{\text{ex}} \rightarrow \bar{J}$ process, in the process $\bar{J} \rightarrow \overline{O}$, a Gaussian nondeterministic channel model, information loss does take place, and the capacity must be computed using the mutual information expression (32). Thus, even while $H(\bar{J})$ is reduced with MC due to the onset of electromagnetically mediated port-to-port statistical correlation (Theorem 2), the conditional entropy $H(\bar{J}|\overline{O})$ is also reduced due to the general information-theoretic inequality $H(X|Y) \leq H(X)$ valid for any two random variables X and Y [53]. Therefore, mutual information (and consequently capacity) may increase or decrease with EM MC. Nevertheless, in general, we expect a degradation of the system performance in rich random scattering environment when MC is present since it introduces

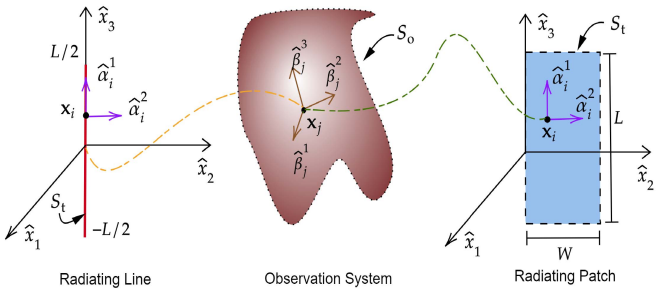

Fig. 2. General configuration of the linear (left) and rectangular (right) radiating systems, both accessed by a measuring apparatus $\mathcal{S}_o$.

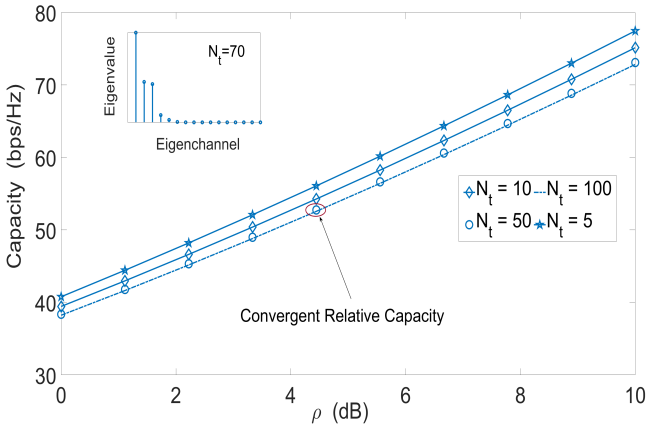

Fig. 3. Capacity convergence results for Example 1.

new correlations.[10] Due to the importance of correlations induced by EM MC, an explicit expression of the correlation matrix in the presence of arbitrary MC was derived, see (62).

V. Numerical Examples and Discussion

In the following examples, the surrounding medium is assumed to be vacuum with no ground plane or scattering objects. In other words, we focus on idealized but fundamental line-of-sight information transmission scenario. The information capacity of a generic surface, however, is strongly dependent in general on the scattering richness of the propagation medium [11], [76]. In this section, our main interest is investigating the impact of the geometry (size and shape) of the radiating surface and the dependence of capacity on the structure of the radiation field, e.g., as per the impact of the distance of the observation apparatus from the radiating current.[11] For definiteness, the following examples are conducted at $f = 2.4\,\text{GHz}$ but the algorithm can be used at any frequency. Finally, in all examples, we set $b_j^r(\omega)$ in (19) to unity for all values $r = 1, 2, 3$, $j = 1, \ldots, N_o$. For further details on the validity of the EM dipole model based on (10), see Remark 3 and the references cited therein.

Example 1 (Far-Field Information Capacity of Dual-Polarized Linear Continuous Source System): Consider a 1-D "surface" S_t consisting of a line oriented along the $\hat{x}_3$-direction, as shown in Fig. 2 (left and center). A set of uncoupled N_t point sources are arranged along the vertical direction with total spatial extension of L. We here examine two possible orthogonal source polarizations physically implemented as two perpendicular small dipoles (cross dipole antenna) based at $\mathbf{x}_i$, with $i = 1, \ldots, N_t$. Each point dipole source's degree of freedom is excited at the same frequency $f = 2.4\,\text{GHz}$. The capacity results of a dual-polarization $\lambda/2$-linear radiator as described above are shown in Fig. 3, which illustrates the convergence behavior of the relative capacity taken with respect to an observation sphere with radius $d = 6\lambda$ (far-field condition) and $N_o = 36$ equally spaced spherical angles (θ, φ) samples. The N_t point sources are uniformly distributed throughout the line extending from $-\lambda/4$ to $\lambda/4$. It can be seen that the relative capacity $C(N_t, N_o)$ saturates with $N_t \to \infty$ and fixed N_o. In particular, no further significant change in capacity was observed to take place for $N_t > 70$, indicating attaining effective convergence of the continuous capacity approximation hierarchy. This suggests the existence of a limit on the information capacity of a $\lambda/2$-continuous source with dual polarization for uncorrelated information point ports (MC-based correlations between the current samples can be always decoupled using proper precoders). In the inset of Fig. 3, we also show the eigenchannels' weights obtained by computing the eigenvalues of the system matrix $\overline{\overline{T}} := \overline{\overline{H}}'^{\dagger}\overline{\overline{H}}'$ for the $N_t = 70$ approximation hierarchy. We can see that only a few effectively independent pathways for transmitting information are available (about 4 or 5). The number of eigenchannels can be increased (and hence the capacity) by inserting random scatterers [76], [78] or reconfigurable intelligent surfaces [32], [34], [84], [85], [86] in order to modify the channel environment.

The impact of polarization, an EM degree of freedom, is one of the oldest and most well-studied aspects in the EM theory of information [11], [87], [88], [89]. In the following example, we use our method to provide a deterministic approach to estimating how this geometrical-physical parameter may influence the information capacity of a continuous source distribution.

Example 2 (Far-Field Capacity Enhancement in Dual-Polarized Continuous Linear Systems): The well-known result about the enhancement of capacity in dual-polarized systems can also be established as a limit of continuous sources by carrying out a convergence analysis similar to Example 1 but with one polarization only allowed. Indeed, Fig. 4 shows the capacity results for $N_t = 75$, whose eigenchannels are shown in the inset of Fig. 3, but this time with the horizontal polarization along the $\hat{x}_2$-direction manually set to zero, while the vertical polarization along the $\hat{x}_3$-direction is left unaffected. It can be seen that the dual-polarization scenario exhibits higher capacity than the single-polarization case. This limit is obtained with infinite number of uncoupled point sources covering the full spatial extension of the $\lambda/2$-radiator, and hence, the difference in capacity shown there is mainly geometrical

[10] If such additional correlations are accounted for, we anticipate that it is still possible to optimize the system performance even in the presence of MC. An investigation of this rather elaborate design problem is outside the scope of the present work.

[11] Since including scattering objects requires extensive side treatment of the physical random scattering models to be used, yet without falling within the stated scope of our article, we relegate scattering effects to future treatments.

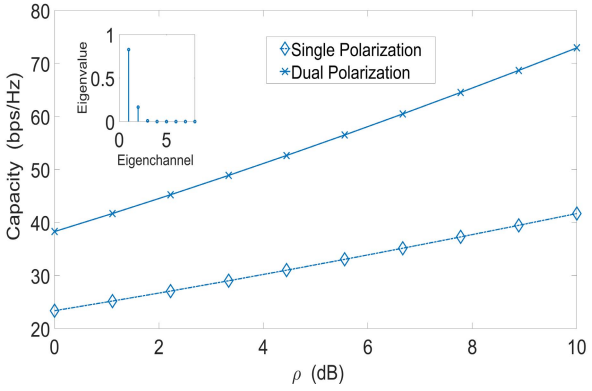

Fig. 4. Capacity convergence results for Example 2.

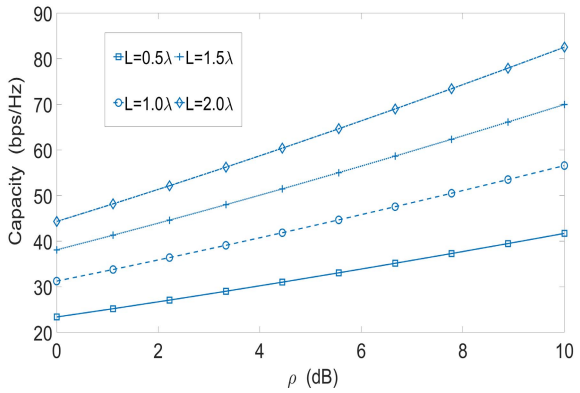

Fig. 5. Linear source far-field capacity results for Example 3. Here, L is the size of the linear source as shown in Fig. 2 (left).

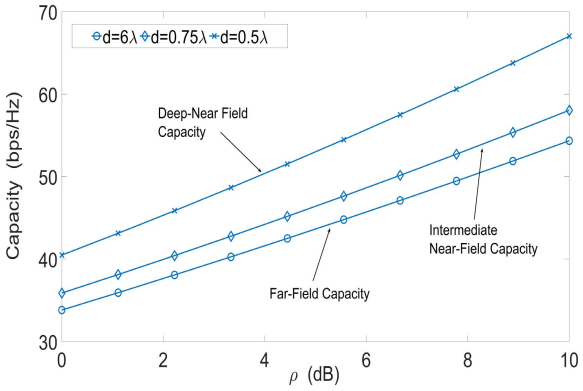

Fig. 6. Linear source NF capacity results for Example 4. Here, d is the radius of the observation sphere $S_o(N_o = 144)$ and the source system has size $L = 0.5\lambda$.

in origin.[12] This reduction in capacity in single-polarization systems can be explained by referring to the eigenchannels weights for the single-polarization case shown in the inset of Fig. 4 and compare it with the corresponding distribution in the inset of Fig. 3. It is clear that the former exhibits a smaller number of independent information pathway transmission compared with the two-polarization configuration, hence the reduction in capacity. The importance of these results stems from the fact they are obtained by a fundamental analysis of the capacity limit of arbitrary linear half-wavelength source distribution, and hence, relative to the current $\mathcal{S}_o(N_o = 36)$ observation system, no further improvement is possible for generic AWGN channels (no knowledge of the exact channel model is available) unless a specialized precoder is used at the excitation point ports [76], [77], [81]. In other words, these limits have their origin in the geometric structure of this problem, i.e., the half-wavelength line source system with spherical field observation in the far-field zone.

Example 3 (Linear Source Far-Field Capacity Enhancement With Respect to Size): At a single frequency, even if we set the MC between point sources to zero, the capacity cannot increase with N_t unless the physical dimensions of the continuous source are increased. In other words, increasing the density of the transmitting point ports does not improve information capacity even when no MC between the point ports takes place with such increase in density. A demonstration of this is shown in Fig. 5 for the case of the linear source of Example 1, where the far-field capacity is varied with the linear source size L. It is clear that higher capacity is obtained for larger electrical size since we kept the same frequency (hence the wavelength) as before. Moreover, to ensure accurate prediction, the number of sources N_t was increased with increasing the radiator size to guarantee that the obtained relative capacity results reasonably approximate continuous source data with respect to the spherical far-field measurement system $\mathcal{S}_o(N_o = 36)$.

Next, we consider the NF analysis of the source system treated in the previous examples. The ability to improve the performance of a communication system by working in the NF zone has already been investigated from multiple viewpoints [90], [91], [92], [93], [94]. Understanding how the information capacity behaves with the distance from the transmitting surface is then important for several applications.

Example 4 (Linear Source NF Capacity): For $L = 0.5\lambda$, the minimum radius of the observation sphere sphere S_o is 0.25λ. We show the far-field results corresponding to $d = 6\lambda$ as well as intermediate and deep NF results in Fig. 6. The number of observation points N_o is increased from 36 in the previous examples to 144. It is clear that NF capacities consistently increase with decreasing receiver distance d, suggesting that NF communication systems enjoy higher information capacity than their far-field counterparts. Theoretically speaking, such increase can be accounted for as being, at least in part, due to the availability of more complex field structure in the NF scenario compared with the FF, where in the latter case, the radial component of the field is zero [93]. Moreover, NF processes possess latent but richer (often evanescent) subwavelength components that can be utilized for encoding extra bits of information [73], [74]. The present method then provides a way to systematically quantify how the geometrical and EM design of the communication system can be modified to maximize the utilization of such latent NF capabilities.

Example 5 (Square Patch NF Relative Capacity Convergence Analysis With Respect to N_t): We consider here a square

[12]However, it should always be recalled that by increasing the number of observation points N_o, one may modify the $N_t \to \infty$ far-field capacity limit. This is why what we are computing here is really the relative capacity as defined in Section IV-B, i.e., the capacity limit taken with respect to a given observation system $\mathcal{S}_o$.

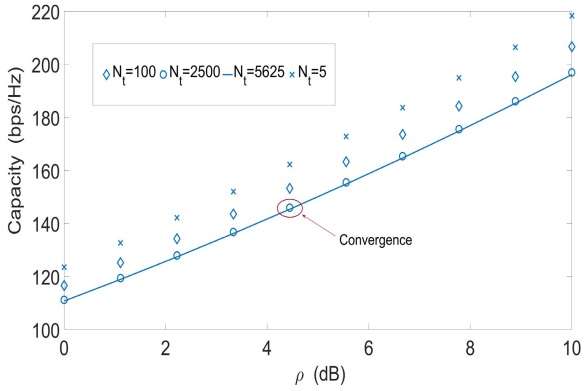

Fig. 7. Square source far-field capacity results for Example 5.

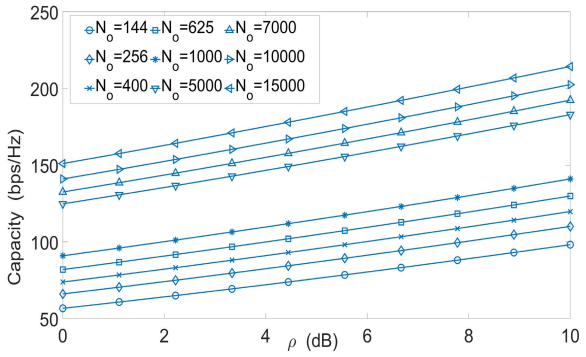

Fig. 8. Square source far-field capacity results for Example 6.

patch with $L = W = 0.5\lambda$ and point sources distributed in the horizontal $\hat{x}_1$- and vertical $\hat{x}_2$-directions of S_t with variable N_t. In the most generic case, there would be two surface polarizations $\hat{\alpha}_i^1 = \hat{x}_1$ and $\hat{\alpha}_i^2 = \hat{x}_2$ (horizontal and vertical polarizations). The point sources are confined to the $\hat{x}_1\hat{x}_2$ plane. In the following results, we choose the point source locations and the associated two polarization directions at each position randomly (using a uniform random variable distribution.) When N_t grows very large, the square patch becomes densely covered with most directions of excitations considered. Our objective here is to investigate the convergence behavior of relative capacity with respect to the fixed observation system S_o when the number of source points N_t increases, while the physical dimensions of the patch are the same. The spherical observation (receive) system is set in the NF zone with radius $d = 1.0\lambda$ and $N_\mathrm{o} = 400$. The capacity results are shown in Fig. 7, where it can be clearly seen that capacity converges to the geometrical limit of a continuous square patch of this electrical size after around 5000 radiating points.

Example 6 (Square Patch Far-Field Relative Capacity Convergence Analysis With Respect to N_o): For a square patch with $L = W = 0.5\lambda$ and 5×5 point sources uniformly distributed in the horizontal and vertical directions of S_t ($N_\mathrm{t} = 25$), we construct a spherical observation (receive) system with radius $d = 50144\lambda$ in order to test the impact of the size of S_o on the convergence of the capacity relative to S_o. We use only one source polarization with $\hat{\alpha}_i^2 = \hat{x}_3$, while the locations $\mathbf{x}_i$ of all point sources are confined to the $\hat{x}_1\hat{x}_2$ plane (vertical polarization). The capacity results are shown in Fig. 8. For such very large sphere, even though the angular span of the spherical observation angles can be well covered with high resolution using few hundreds angular point samples, the minimum physical distance between nearby point receivers on S_o is proportional to $d\mathrm{d}\Omega$, which is significant for very large d even when the angle $\mathrm{d}\Omega$ between two points is very small. This implies that the underlying MIMO system can still improve the information capacity as the results clearly shown in Fig. 8. Due to computer memory limitation, with such massive radius d, it is not possible to simulate an arbitrarily large number of receiver points in order to estimate the convergence of Shannon capacity relative to $S_\mathrm{o}(N_\mathrm{o} \to \infty)$. With smaller d, one can obtain convergent relative capacity when N_t and N_o becomes large enough. It should be noted though that while capacity was increasing with N_o, the rank of $\overline{\overline{H}}$ and the weights of the system eigenchannels converge rapidly. This suggests that the information channel quickly stabilizes with increasing N_o and approaches the far-field transmission capabilities of the radiating array under consideration. All extra gains in capacity observed in Fig. 8 with increasing N_o are due to the high minimum critical density of receive points needed on a sphere with very large radius d in order to approximate a continuous receiver. Again, these observations can be confirmed by rerunning this example with observation spheres with small radius.

Examples 5 and 6 also suggest taking extra care in calculating the NF capacity using the IDM approach based on the MIMO system capacity. The reason is that it is known that if the number of dipoles is small (between 5 and 10), then the validity of the NF formula is restricted to a distance about λ from the radiating surface [61]. For accurate predictions of the NF capacity, it is required that one takes the $N_\mathrm{t} \to \infty$ limit before the distance limit. In other words, if $C(N_\mathrm{t}, N_\mathrm{o}, d)$ is the capacity of a radiating $S_\mathrm{t}(N_\mathrm{t})$ measured by spherical $S_\mathrm{o}(N_\mathrm{o})$ system with radius d, then we note that the following situation holds:

$$\lim_{d\to 0}\lim_{N_\mathrm{t}\to\infty} C(N_\mathrm{t}, N_\mathrm{o}, d) \neq \lim_{N_\mathrm{t}\to\infty}\lim_{d\to 0} C(N_\mathrm{t}, N_\mathrm{o}, d). \quad (45)$$

Stated differently, due to the discrete nature of our original EM model, limit operations should be approached very carefully since the underlying process involves continuous quantities. However, we define the deep NF capacity relative to a shrinking spherical surface with N_o observation points by an expression of the form

$$C_\mathrm{NF}(N_\mathrm{o}) := \lim_{d\to 0}\lim_{N_\mathrm{t}\to\infty} C(N_\mathrm{t}, N_\mathrm{o}, d). \quad (46)$$

In this way, the shortcoming of the dipole model can be avoided since it is known that a large enough number of dipoles can capture very well the structure of the NF even with strong MC [66]. A complete rigorous theory bypassing restrictions such as (45) is outside the scope of the present work.

Example 7 (Spherical Far-Field and NF Relative Capacity Performance Analysis With MC): In this example, we study a nonplanner radiating surface, a sphere with radius a, and

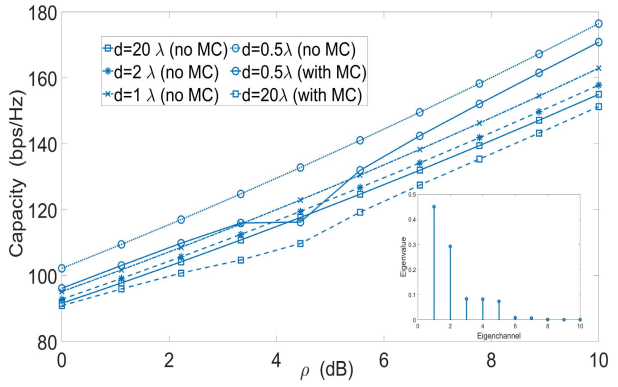

Fig. 9. Spherical far-field and NF capacity performance analysis for Example 7. The inset provides the eigenchannel weights for the MC case of correlated (with random MC) point sources when the observation sphere is in the far zone ($d = 20\lambda$).

compute both its far-field and NF capacities using a spherical observation system (see Fig. 1). The far-field capacity of a transmitting spherical surface with $a = 0.1\lambda$ is shown in Fig. 9, where the observation sphere is located at distance d and we choose $N_{\rm t} = N_{\rm o} = 360$. In order to illustrate how capacity in such basic system depends on distance, several simulations were conducted with variable d, where the far-field case corresponds to the largest distance $d = 20\lambda$. Again, we notice the overall pattern of increasing capacity when the distance of the receiver to the transmitter is reduced. For the case of MC, we assume a real random correlation matrix $\overline{\overline{C}}_{\bar{J}}$ of the form $\overline{\overline{C}}_{\bar{J}} = \sigma_{\bar{J}}^2 A$, where A is a $2N_{\rm t} \times 2N_{\rm t}$ random matrix whose entries are uniformly distributed random variables between 0 and 1. We give two examples with MC, one for the far-field ($d = 20\lambda$) and the other for the deep NF ($d = 0.5\lambda$). The results labeled "with MC" in Fig. 9 correspond to two different instantiations of such MC/source correlation scenario. In these numerical experiments, it is found that the capacity with MC is less than the corresponding capacity without MC.

VI. Conclusion

We introduced a general method to define and compute useful information capacity measures for generic radiating surfaces, with possible applications as transmitters or reconfigurable reflecting surfaces that might be deployed in wireless communication systems. Various computational examples were provided, including 1-D and 2-D transmitting systems with various polarization degrees of freedom. The far-field capacity was computed and it was found that the capacity relative to a given observation surface converges with increasing $N_{\rm t}$. Moreover, we computed the capacity as a function of the distance from the source and found that NF capacity consistently outperforms the far-field capacity. Some examples were given where the stochastic correlation between induced radiating current elements, caused by EM MC, influenced the capacity of a spherical transmitting surface. The proposed method works for both planer and curved structures and can be used in future research on how to design optimized capacity-driven EM communication systems. Moreover, our approach can be integrated with existing full-wave EM CAD tools in order to supply the Shannon information capacity data for familiar antenna array systems used in prototyping and designing current or future wireless communication systems.

The theory developed here and its computational algorithm can be further developed and expanded in future works. For example, it may be interesting to generalize the observation process $S_{\rm o}$ to real-life measurement scenarios by allowing for some correlation between measurement probes and, hence, measurement noise. One may also consider the impact of corners (diffraction effects), scattering clusters, nearby objects, and so on on the communication channel. The detailed optimization results may be provided to design a high-capacity driven communication link exploiting the presence of EM MC and related correlation processes.

Appendix A
On Mathematical Notation

This article uses a formalism that combines methods and notations often deployed in two distinct fields, EM theory, and information theory. For that reason, some tensions in our use of various notations may naturally arise. To avoid any confusion, we attempted to explain the meaning of the notation within the main text. For ease of reference, the Nomenclature provides a complete list of all notations utilized in writing this article. In particular, we consistently distinguish between a dyad and a matrix array. In addition, throughout this article, we drop explicit frequency dependence whenever no confusion may arise.

Appendix B
Channel Matrix Normalization and the Definition of Signal-to-Noise Ratio

The physical channel matrix $\overline{\overline{H}}$ in (31) can be renormalized by rewriting the field observable vector in the following slightly different form:

$$\overline{O}(\omega) = \alpha \overline{\overline{H}}'(\omega) \cdot \bar{J}(\omega) + \overline{n}, \quad \overline{\overline{H}}' := \frac{1}{\alpha}\overline{\overline{H}} \tag{47}$$

where $\alpha \in \mathbb{R}^+$ is a normalization factor and $\overline{\overline{H}}'$ is the normalized channel matrix. In terms of this model, the total received power can be computed, yielding

$$\begin{aligned} P_{\rm rx,tot} &= \mathbb{E}\left\{\overline{O} \cdot \overline{O}^{\dagger}\right\} \\ &= \alpha^2\sigma_J^2 {\rm Tr}\overline{\overline{H}}' \cdot \overline{\overline{H}}'^{\dagger} + \sigma_n^2 {\rm Tr}\{\mathbb{1}_{3N_{\rm o}}\} \\ &= \alpha^2\sigma_J^2 \left\|\overline{\overline{H}}'\right\|_F^2 + 3N_{\rm o}\sigma_n^2 \end{aligned} \tag{48}$$

where $\| \ \|_F$ stands for the Frobenius norm and Tr stands for the matrix trace operation. Thus, the ratio of total measured power relative to the total noise power at the observation surface $S_{\rm o}$ can be estimated as

$$\rho = \frac{\alpha^2\sigma_J^2 \left\|\overline{\overline{H}}'\right\|_F^2}{3N_{\rm o}\sigma_n^2}. \tag{49}$$

We impose the following normalization conditions:

$$\alpha = \sqrt{\rho}, \quad \left\|\overline{\overline{H}}'\right\|_F^2 = 1. \tag{50}$$

Using (47) in (36) leads to the following spectral efficiency expression:

$$C = 2\log\det\left[\mathbb{1}_{2N_\mathrm{t}} + \alpha^2\frac{\sigma_J^2}{\sigma_n^2}\,\overline{\overline{H}}'^{\dagger}\cdot\overline{\overline{H}}'\right]. \tag{51}$$

Applying (49) and (50) to (51), formula (37) is obtained.

Appendix C
On the Relationship Between the Excitation Field Correlation Matrix, EM MC, and Mutual Information

Consider a transmitting system $\mathcal{S}_\mathrm{t}$ with N_t excitation points distributed at $\mathbf{x}_i, i = 1,\ldots,N_\mathrm{t}$. Ultimate information source excitations can be traced back to the external field column array

$$\overline{E}^{\mathrm{ex}} := \left[\overline{E}_i^{\mathrm{ex}}\right]_{i=1}^{N_\mathrm{t}}, \quad \overline{E}_i^{\mathrm{ex}} := \begin{bmatrix}E_{i,1}^{\mathrm{ex}} & E_{i,2}^{\mathrm{ex}}\end{bmatrix}^T \tag{52}$$

where

$$\overline{E}_i^{\mathrm{ex}} = \hat{\alpha}_i^1 E_{i,1}^{\mathrm{ex}} + \hat{\alpha}_i^2 E_{i,2}^{\mathrm{ex}}, \quad E_{is}^{\mathrm{ex}} := E_s^{\mathrm{ex}}(\mathbf{x}_i), \quad s = 1,2 \tag{53}$$

is the ith component (point port) excitation field tangential to the surface S_t at $\mathbf{x}_i$, while we recall that $\hat{\alpha}_i^s := \hat{\alpha}^s(\mathbf{x}_i), s = 1,2$. The excitation field point-port array $\overline{E}^{\mathrm{ex}}$ generates the corresponding array of currents $\bar{J}$ defined by (25). Our goal is to investigate the relation between MC and the statistics of these two arrays in light of the information-theoretic framework of the capacity formula (34).

We first note that in the frequency domain, the spatiotemporal relation (5) reduces into [19], [95]

$$\mathbf{J}(\mathbf{x},\omega) = \int_{S_\mathrm{t}} \mathrm{d}s'\overline{\mathbf{F}}(\mathbf{x},\mathbf{x}',\omega)\cdot\mathbf{E}^{\mathrm{ex}}(\mathbf{x}',\omega) \tag{54}$$

with

$$\overline{\mathbf{F}}(\mathbf{x},\mathbf{x}',\omega) = \sum_{s=1}^{2}\sum_{s'=1}^{2}\hat{\alpha}^s(\mathbf{x})\otimes\hat{\alpha}^{s'}(\mathbf{x}')F(\mathbf{x},\mathbf{x}';\omega). \tag{55}$$

The excitation field corresponding to (16) can be written as

$$\mathbf{E}(\mathbf{x}',\omega;\mathcal{S}_\mathrm{t}) = \sum_{i'=1}^{N_\mathrm{t}}\sum_{s'=1}^{2}\hat{\alpha}_{i'}^{s'}E_{i's'}^{\mathrm{ex}}(\omega)\delta_S(\mathbf{x}'-\mathbf{x}_{i'}) \tag{56}$$

where δ_S is a surface Dirac delta function as defined in [19] and [60]. Substituting (56) into (54), using (55), we find

$$\mathbf{J}(\mathbf{x},\omega) = \sum_{s=1}^{2}\sum_{i'=1}^{N_\mathrm{t}}\sum_{s'=1}^{2}\hat{\alpha}^s(\mathbf{x})F^{ss'}(\mathbf{x},\mathbf{x}_{i'};\omega)E_{i's'}^{\mathrm{ex}}(\omega). \tag{57}$$

If we choose to sample the radiating current at the same locations as $\mathbf{x}_{i'}, i' = 1,\ldots,N_\mathrm{t}$, then the obtained current samples $\mathbf{J}_i := \mathbf{J}(\mathbf{x}_i,\omega)$ may be expressed as

$$\mathbf{J}_i(\omega) = \sum_{s=1}^{2}\sum_{i'=1}^{N_\mathrm{t}}\sum_{s'=1}^{2}\hat{\alpha}_i^s F_{ii'}^{ss'}(\omega)E_{i's'}^{\mathrm{ex}}(\omega) \tag{58}$$

where

$$F_{ii'}^{ss'}(\omega) := F^{ss'}(\mathbf{x}_i,\mathbf{x}_{i'};\omega), \quad i,i' = 1,\ldots,N_\mathrm{t}. \tag{59}$$

Therefore, the ith current sample is a linear combination of the excitation signals at all other point ports indexed by i'. This is the most general form of the N_t-point-port approximation of the continuous transmitting surface S_t.

The radiating current on the transmitting surface possesses a correlation matrix $\overline{\overline{C}}_{\bar{J}}$ of the form (29). Let the average values of the excitation signals all be zero, i.e., assume $\mathbb{E}[E_{is}^{\mathrm{ex}}] = 0$ for all i and s. It then follows from (58) that $\mathbb{E}[J_i] = 0$ as well. It is not difficult to see that through suitable matrix partitioning operations, $\overline{\overline{C}}_{\bar{J}}$ can be put into the following general structure:

$$\overline{\overline{C}}_{\bar{J}}(\omega) = \begin{bmatrix}\overline{\overline{C}}_{\bar{J}}^{11}(\omega) & \cdots & \overline{\overline{C}}_{\bar{J}}^{1N_\mathrm{t}}(\omega)\\ \vdots & \ddots & \vdots\\ \overline{\overline{C}}_{\bar{J}}^{N_\mathrm{t}1}(\omega) & \cdots & \overline{\overline{C}}_{\bar{J}}^{N_\mathrm{t}N_\mathrm{t}}(\omega)\end{bmatrix}_{N_\mathrm{t}\times N_\mathrm{t}} \tag{60}$$

where

$$\overline{\overline{C}}_{\bar{J}}^{i_1i_2} := \begin{bmatrix}C_{\bar{J}}^{i_1i_2,11}(\omega) & C_{\bar{J}}^{i_1i_2,12}(\omega)\\ C_{\bar{J}}^{i_1i_2,21}(\omega) & C_{\bar{J}}^{i_1i_2,22}(\omega)\end{bmatrix}_{2\times 2}. \tag{61}$$

In order to find an explicit formula for the matrix entries, we substitute (58) into (29), performing some straightforward manipulations, arriving at

$$C_{\bar{J}}^{i_1i_2s_1s_2} = \sum_{i_1',i_2'=1}^{N_\mathrm{t}}\sum_{s_1',s_2'=1}^{2}F_{i_1i_1'}^{s_1s_1'}\left(F_{i_2i_2'}^{s_2s_2'}\right)^*\mathbb{E}\left[E_{i_1's_1'}^{\mathrm{ex}}\left(E_{i_2's_2'}^{\mathrm{ex}}\right)^*\right] \tag{62}$$

where $i_1,i_2 = 1,\ldots,N_\mathrm{t}$ and $s_1,s_2 = 1,2$. Expression (62) relates the correlation between the radiating current samples to cross correlation phenomena as seen at the point-port excitation field locations. In particular, Theorems 1 and 2 immediately follow from (62).

Furthermore, note the nonlocal nature of the relation where the correlation between any pair of current samples depends on cross correlation between the field values samples at all other corresponding excitation field position pairs. Most importantly though, even when the field excitations are uncorrelated, relation (62) shows that the current samples remain correlated as long as the EM coupling Green's functions coefficients, here the array (59), are not negligible.

References

[1] L. Brillouin, *Science and Information Theory* (Dover Books on Physics), 2nd ed. Mineola, NY, USA: Dover, Jul. 2013.

[2] D. Gabor, "Theory of communication. Part 1: The analysis of information," *J. Inst. Elect. Eng., Radio Commun. Eng.*, vol. 93, no. 26, pp. 429–441, Nov. 1946.

[3] M. Franceschetti, S. Marano, and F. Palmieri, "The role of entropy in wave propagation," in *Proc. IEEE Int. Symp. Inf. Theory*, Jun. 2003, p. 251.

[4] F. K. Gruber and E. A. Marengo, "New aspects of electromagnetic information theory for wireless and antenna systems," *IEEE Trans. Antennas Propag.*, vol. 56, no. 11, pp. 3470–3484, Nov. 2008.

[5] M. D. Migliore, "On electromagnetics and information theory," *IEEE Trans. Antennas Propag.*, vol. 56, no. 10, pp. 3188–3200, Oct. 2008.

[6] M. Franceschetti, "Wave diversity limits for wireless communication," in *Proc. IEEE Antennas Propag. Soc. Int. Symp.*, Jul. 2008, pp. 1–4.

[7] S. Mikki, "The antenna spacetime system theory of wireless communications," *Proc. Roy. Soc. A, Math., Phys. Eng. Sci.*, vol. 475, no. 2224, Apr. 2019, Art. no. 20180699.

[8] M. T. Ivrlac and J. A. Nossek, "Toward a circuit theory of communication," *IEEE Trans. Circuits Syst. I, Reg. Papers*, vol. 57, no. 7, pp. 1663–1683, Jul. 2010.

[9] W. Geyi, "Capacity of transmitting antenna," in *Proc. IEEE Antennas Propag. Soc. Int. Symp.*, Jun. 2007, pp. 4052–4055.

[10] S. M. Mikki and Y. Antar, "Unifying electromagnetic and communication theories: A proposal for a new research program," in *Proc. URSI Int. Symp. Electromagn. Theory (EMTS)*, Aug. 2016, pp. 435–438.

[11] W. C. Jake, *Microwave Mobile Communications* (An IEEE Press Classic Reissue). Hoboken, NJ, USA: Wiley, 1994.

[12] A. M. Tulino, A. Lozano, and S. Verdú, "Impact of antenna correlation on the capacity of multiantenna channels," *IEEE Trans. Inf. Theory*, vol. 51, no. 7, pp. 2491–2509, Jul. 2005.

[13] J. W. Wallace and M. A. Jensen, "Statistical characteristics of measured MIMO wireless channel data and comparison to conventional models," in *Proc. IEEE 54th Veh. Technol. Conf. VTC Fall.*, Oct. 2001, pp. 1078–1082.

[14] R. Vaughan and J. B. B. Andersen, *Channels, Propagation and Antennas for Mobile Communications* (Electromagnetics and Radar). London, U.K.: Institution of Engineering and Technology, 2003.

[15] S. M. Mikki and Y. M. M. Antar, "On cross correlation in antenna arrays with applications to spatial diversity and MIMO systems," *IEEE Trans. Antennas Propag.*, vol. 63, no. 4, pp. 1798–1810, Apr. 2015.

[16] S. M. Mikki, S. Clauzier, and Y. M. M. Antar, "A correlation theory of antenna directivity with applications to superdirective arrays," *IEEE Antennas Wireless Propag. Lett.*, vol. 18, no. 5, pp. 811–815, May 2019.

[17] D. Sarkar, S. M. Mikki, and Y. M. M. Antar, "An efficient analytical evaluation of the electromagnetic cross correlation Green's function in MIMO systems," *IEEE Trans. Antennas Propag.*, vol. 67, no. 11, pp. 6947–6956, Nov. 2019.

[18] M. Franceschetti, *Wave Theory of Information*. Cambridge, U.K.: Cambridge Univ. Press, 2012.

[19] S. M. Mikki and Y. M. M. Antar, "The antenna current Green's function formalism—Part I," *IEEE Trans. Antennas Propag.*, vol. 61, no. 9, pp. 4493–4504, Sep. 2013.

[20] S. M. Mikki and Y. M. M. Antar, "The antenna current Green's function formalism—Part II," *IEEE Trans. Antennas Propag.*, vol. 61, no. 9, pp. 4505–4519, Sep. 2013.

[21] J. W. Wallace and M. A. Jensen, "Intrinsic capacity of the MIMO wireless channel," in *Proc. IEEE 56th Veh. Technol. Conf.*, vol. 2, 2002, pp. 701–705.

[22] A. Martini, A. Massa, and M. Franceschetti, "Physical limits to the capacity of wide-band Gaussian MIMO channels," *IEEE Trans. Wireless Commun.*, vol. 8, no. 7, pp. 3396–3400, Jul. 2009.

[23] S. Mikki and A. Hanoon, "Spectral efficiency enhancement using an antenna-based orthogonal frequency division multiaccess technique," *Int. J. RF Microw. Comput.-Aided Eng.*, vol. 30, no. 11, Nov. 2020, Art. no. e22404.

[24] S. Lu, H. T. Hui, and M. Bialkowski, "Optimizing MIMO channel capacities under the influence of antenna mutual coupling," *IEEE Antennas Wireless Propag. Lett.*, vol. 7, pp. 287–290, 2008.

[25] B. Rohani, K. Takahashi, H. Arai, Y. Kimura, and T. Ihara, "Improving channel capacity in indoor 4×4 MIMO base station utilizing small bidirectional antenna," *IEEE Trans. Antennas Propag.*, vol. 66, no. 1, pp. 393–400, Jan. 2018.

[26] S. Saab, A. Mezghani, and R. W. Heath, "Capacity based optimization of compact wideband antennas," in *Proc. IEEE-APS Topical Conf. Antennas Propag. Wireless Commun. (APWC)*, Sep. 2019, pp. 322–325.

[27] N. Chiurtu and B. Rimoldi, "Varying the antenna locations to optimize the capacity of multi-antenna Gaussian channels," in *Proc. IEEE Int. Conf. Acoust., Speech, Signal Process.*, vol. 5, Jun. 2000, pp. 3121–3123.

[28] I. Yoo, M. F. Imani, T. Sleasman, H. D. Pfister, and D. R. Smith, "Enhancing capacity of spatial multiplexing systems using reconfigurable cavity-backed metasurface antennas in clustered MIMO channels," *IEEE Trans. Comms.*, vol. 67, no. 2, pp. 1070–1084, Feb. 2019.

[29] V. J. Bladel, *Electromagnetic Fields*. Hoboken, NJ, USA: Wiley, 2007.

[30] C. A. Balanis, *Antenna Theory: Analysis and Design*, 4th ed. Hoboken, NJ, USA: Wiley, 2015.

[31] A. Almohamad et al., "Smart and secure wireless communications via reflecting intelligent surfaces: A short survey," *IEEE Open J. Commun. Soc.*, vol. 1, pp. 1442–1456, 2020.

[32] M. Di Renzo et al., "Smart radio environments empowered by reconfigurable intelligent surfaces: How it works, state of research, and the road ahead," *IEEE J. Sel. Areas Commun.*, vol. 38, no. 11, pp. 2450–2525, Jul. 2020.

[33] D. Sarkar, S. Mikki, and Y. M. M. Antar, "Engineering the eigenspace structure of massive MIMO links through frequency-selective surfaces," *IEEE Antennas Wireless Propag. Lett.*, vol. 18, no. 12, pp. 2701–2705, Dec. 2019.

[34] J. C. B. Garcia, A. Sibille, and M. Kamoun, "Reconfigurable intelligent surfaces: Bridging the gap between scattering and reflection," *IEEE J. Sel. Areas Commun.*, vol. 38, no. 11, pp. 2538–2547, Nov. 2020.

[35] R. G. Gallager, *Information Theory and Reliable Communication*. Nashville, TN, USA: Wiley, Jan. 1968.

[36] R. J. Adler and J. Taylor, *Random Fields and Geometry* (Monographs in Mathematics). New York, NY, USA: Springer, Jun. 2007.

[37] S. Mikki and J. Aulin, "The stochastic electromagnetic theory of antenna-antenna cross-correlation in MIMO systems," in *Proc. 12th Eur. Conf. Antennas Propag. (EuCAP)*, 2018, pp. 1–5.

[38] A. Ishimaru, *Wave Propagation and Scattering in Random Media*. New York, NY, USA: Oxford Univ. Press, 1997.

[39] N. Costa and S. Haykin, *Multiple-Input, Multiple-Output Channel Models: Theory and Practice*. Hoboken, NJ, USA: Wiley, 2010.

[40] R. Heath and A. Lozano, *Foundations of MIMO Communication*. Cambridge, U.K.: Cambridge Univ. Press, 2019.

[41] S. Cohen and R. J. Elliott, *Stochastic Calculus and Applications*. New York, NY, USA: Birkhauser, 2015.

[42] J.-F. Le Gall, *Brownian Motion, Martingales, and Stochastic Calculus* (Graduate Texts in Mathematics). New York, NY, USA: Springer, May 2018.

[43] W. C. Gibson, *The Method of Moments in Electromagnetics*. Boca Raton, FL, USA: CRC Press, 2015.

[44] H. Harmuth, *Antennas and Waveguides for Nonsinusoidal Waves*. Orlando, Florida: Academic Press, 1984.

[45] L. B. B. Felsen, *Electromagnetic Field Computation by Network Methods*. Berlin, Germany: Springer, 2010.

[46] R. E. Collin, *Field Theory of Guided Waves*. Hoboken, NJ, USA: Wiley, 1991.

[47] D. Colton and R. Kress, *Inverse Acoustic and Electromagnetic Scattering Theory*. Cham, Switzerland: Springer, 2019.

[48] J.-C. Nedelec, *Acoustic and Electromagnetic Equations: Integral Representations for Harmonic Problems*. New York, NY, USA: Springer, 2001.

[49] S. Mikki and Y. Antar, *New Foundations for Applied Electromagnetics: The Spatial Structure of Fields*. London, U.K.: Artech House, 2016.

[50] J. Schwinger, *Classical Electrodynamics*. New York, NY, USA: Perseus Books, 1998.

[51] L. Felsen, *Radiation and Scattering of Waves*. Piscataway, NJ, USA: IEEE Press, 1994.

[52] C.-T. Tai, *Dyadic Green Functions in Electromagnetic Theory*. Piscataway, NJ, USA: IEEE Press, 1994.

[53] T. M. Cover and J. A. Thomas, *Elements of Information Theory*. Hoboken, NJ, USA: Wiley-Interscience, 2006.

[54] M. Nielsen and I. L. Chuang, *Quantum Computation and Quantum Information*. Cambridge, U.K.: Cambridge Univ. Press, 2010.

[55] M. Wilde, *Quantum Information Theory*. Cambridge, U.K.: Cambridge Univ. Press, 2017.

[56] W. Geyi, *Foundations of Applied Electrodynamics*. Hoboken, NJ, USA: Wiley, 2010.

[57] L. D. Landau and E. Lifshitz, *Electrodynamics of Continuous Media*. Oxford U.K.: Butterworth-Heinemann, 1984.

[58] W. Appel, *Mathematics for Physics and Physicists*. Princeton, NJ, USA: Princeton Univ. Press, 2007.

[59] L. Schwartz, *Mathematics for the Physical Sciences*. Mineola, NY, USA: Dover, 2008.

[60] S. Mikki, "Generalized current Green's function formalism for electromagnetic radiation by composite systems," *Prog. Electromagn. Res. B*, vol. 87, pp. 171–191, 2020.

[61] S. M. Mikki and A. A. Kishk, "Theory and applications of infinitesimal dipole models for computational electromagnetics," *IEEE Trans. Antennas Propag.*, vol. 55, no. 5, pp. 1325–1337, May 2007.

[62] S.-J. Yang, Y.-D. Kim, H.-W. Jo, and N.-H. Myung, "Alternative method for obtaining antenna current Green's function based on infinitesimal dipole modeling," *IEEE Trans. Antennas Propag.*, vol. 67, no. 4, pp. 2583–2590, Apr. 2019.

[63] Y.-D. Kim, H.-J. Kim, K.-U. Bae, J.-H. Park, and N.-H. Myung, "A hybrid UTD-ACGF technique for DOA finding of receiving antenna array on complex environment," *IEEE Trans. Antennas Propag.*, vol. 63, no. 11, pp. 5045–5055, Nov. 2015.

[64] Y.-D. Kim, D.-W. Yi, S.-J. Yang, H. Chae, J.-W. Yu, and N.-H. Myung, "Beam pattern analysis of antenna array on complex platform using AEP method based on hybrid UTD-ACGF technique," *IEEE Trans. Antennas Propag.*, vol. 65, no. 3, pp. 1511–1516, Mar. 2017.

[65] I. A. Baratta, C. B. De Andrade, R. R. De Assis, and E. J. Silva, "Infinitesimal dipole model using space mapping optimization for antenna placement," *IEEE Antennas Wireless Propag. Lett.*, vol. 17, no. 1, pp. 17–20, Jan. 2018.
[66] S. M. Mikki and Y. M. M. Antar, "Near-field analysis of electromagnetic interactions in antenna arrays through equivalent dipole models," *IEEE Trans. Antennas Propag.*, vol. 60, no. 3, pp. 1381–1389, Mar. 2012.
[67] J.-I. Oh, S. J. Yang, S. Kim, J.-W. Yu, and Y. D. Kim, "Antenna diagnostics based on infinitesimal dipole modeling with limited measurement on antenna aperture," *IEEE Antennas Wireless Propag. Lett.*, vol. 21, no. 5, pp. 923–927, May 2022.
[68] J. F. Izquierdo, J. Rubio, and J. Zapata, "Antenna-generalized scattering matrix in terms of equivalent infinitesimal dipoles: Application to finite array problems," *IEEE Trans. Antennas Propag.*, vol. 60, no. 10, pp. 4601–4609, Oct. 2012.
[69] S. Clauzier, S. M. Mikki, and Y. M. M. Antar, "Design of high-diversity gain MIMO antenna arrays through surface current optimization," in *Proc. IEEE Int. Symp. Antennas Propag. USNC/URSI Nat. Radio Sci. Meeting*, Oct. 2015, pp. 9–10.
[70] S. Clauzier, S. M. Mikki, Y. M. M. Antar, A. Sharaiha, and P. Pouliguen, "A method to obtain current distributions on small antennas with optimum directivity," in *Proc. IEEE Int. Symp. Antennas Propag. USNC/URSI Nat. Radio Sci. Meeting*, Jul. 2015, pp. 1406–1407.
[71] S. Clauzier, S. M. Mikki, and Y. M. M. Antar, "Design of near-field synthesis arrays through global optimization," *IEEE Trans. Antennas Propag.*, vol. 63, no. 1, pp. 151–165, Jan. 2015.
[72] S. M. Mikki and Y. M. M. Antar, "Analysis of generic near-field interactions using the antenna current Green's function," *Prog. Electromagn. Res. C*, vol. 59, pp. 1–9, 2015.
[73] S. M. Mikki and Y. M. M. Antar, "A theory of antenna electromagnetic near field—Part I," *IEEE Trans. Antennas Propag.*, vol. 59, no. 12, pp. 4691–4705, Dec. 2011.
[74] S. M. Mikki and Y. M. M. Antar, "A theory of antenna electromagnetic near field—Part II," *IEEE Trans. Antennas Propag.*, vol. 59, no. 12, pp. 4706–4724, Dec. 2011.
[75] T. Hansen and A. D. Yaghjian, *Plane-Wave Theory of Time-Domain Fields: Near-Field Scanning applications*. New York, NY, USA: IEEE Press, 1999.
[76] J. Hampton, *Introduction to MIMO Communications*. Cambridge, U.K.: Cambridge Univ. Press, 2013.
[77] T. L. Marzetta, E. G. Larsson, H. Yang, and H. Q. Ngo, *Fundamentals of Massive MIMO*. Cambridge, U.K.: Cambridge Univ. Press, 2016.
[78] E. Telatar, "Capacity of multi-antenna Gaussian channels," *Eur. Trans. Telecommun.*, vol. 10, no. 6, pp. 585–595, Feb. 1999.
[79] A. Hanoon and S. Mikki, "Bandwidth-enhancement of digital communication systems employing narrowband antennas: A novel electromagnetic OFDM approach," in *Proc. IEEE Int. Symp. Antennas Propag. USNC/URSI Nat. Radio Sci. Meeting*, Jul. 2017, pp. 527–528.
[80] A. Oppenheim and R. Schafer, *Discrete-Time Signal Processing*. Upper Saddle River, NJ, USA: Pearson, 2010.
[81] B. P. Lathi and Z. Ding, *Modern Digital and Analog Communication Systems*. New York, NY, USA: Oxford Univ. Press, 2019.
[82] A. A. Abouda and S. Häggman, "Effect of mutual coupling on capacity of MIMO wireless channels in high SNR scenario," *Prog. Electromagn. Res.*, vol. 65, pp. 27–40, 2006.
[83] R. Janaswamy, "Effect of element mutual coupling on the capacity of fixed length linear arrays," *IEEE Antennas Wireless Propag. Lett.*, vol. 1, pp. 157–160, 2002.
[84] E. Basar, "Reconfigurable intelligent surface-based index modulation: A new beyond MIMO paradigm for 6G," *IEEE Trans. Commun.*, vol. 68, no. 5, pp. 3187–3196, May 2020.
[85] A.-A. A. Boulogeorgos and A. Alexiou, "Performance analysis of reconfigurable intelligent surface-assisted wireless systems and comparison with relaying," *IEEE Access*, vol. 8, pp. 94463–94483, 2020.
[86] D. Sarkar, S. Mikki, and Y. Antar, "An electromagnetic framework for the deployment of reconfigurable intelligent surfaces to control massive MIMO channel characteristics," in *Proc. 14th Eur. Conf. Antennas Propag. (EuCAP)*, Mar. 2020, pp. 1–4.
[87] P. Kyritsi, D. C. Cox, R. A. Valenzuela, and P. W. Wolniansky, "Effect of antenna polarization on the capacity of a multiple element system in an indoor environment," *IEEE J. Sel. Areas Commun.*, vol. 20, no. 6, pp. 1227–1239, Aug. 2002.
[88] B. Lee et al., "Modeling the indoor channel for the MIMO system using dual polarization antennas," in *Proc. Eur. Conf. Wireless Technol.*, 2006, pp. 334–337.
[89] P.-Y. Qin, Y. J. Guo, and C.-H. Liang, "Effect of antenna polarization diversity on MIMO system capacity," *IEEE Antennas Wireless Propag. Lett.*, vol. 9, pp. 1092–1095, 2010.
[90] H. Hirayama, G. Matsui, N. Kikuma, and K. Sakakibara, "Improvement of channel capacity of near-field MIMO," in *Proc. 4th Eur. Conf. Antennas Propag.*, 2010, pp. 1–4.
[91] S. Phang, M. T. Ivrlac, G. Gradoni, S. C. Creagh, G. Tanner, and J. A. Nossek, "Near-field MIMO communication links," *IEEE Trans. Circuits Syst. I, Reg. Papers*, vol. 65, no. 9, pp. 3027–3036, Sep. 2018.
[92] R. Zhu, J. Zhou, G. Jiang, and Q. Fu, "Range migration algorithm for near-field MIMO-SAR imaging," *IEEE Geosci. Remote Sens. Lett.*, vol. 14, no. 12, pp. 2280–2284, Dec. 2017.
[93] S. Mikki, "Theory of nonsinusoidal antennas for near-field communication system analysis," *Prog. Electromagn. Res.*, vol. 86, pp. 177–193, 2020.
[94] S. Zhao, Q. Li, Q. Zhang, and J. Qin, "Antenna selection for simultaneous wireless information and power transfer in MIMO systems," *IEEE Commun. Lett.*, vol. 18, no. 5, pp. 789–792, May 2014.
[95] S. M. Mikki and Y. M. M. Antar, "On the fundamental relationship between the transmitting and receiving modes of general antenna systems: A new approach," *IEEE Antennas Wireless Commun. Lett.*, vol. 11, pp. 232–235, 2012.

Said Mikki is an Associate Professor of electrical engineering with the Zhejiang University/University of Illinois at Urbana–Champaign (ZJU-UIUC) Institute, China. His current research interests are focused on quantum engineering, electromagnetics, information theory, and artificial intelligence.